Interface Focus

Interface Focus (2011) **1**, 576–601
doi:10.1098/rsfs.2011.0037
Published online 8 June 2011

REVIEW

Micro-ultrasound for preclinical imaging

F. Stuart Foster[1,*], John Hossack[2] and S. Lee Adamson[3]

[1]*Sunnybrook and Health Sciences Centre, and* [3]*Mt Sinai Hospital, Department of Medical Biophysics, University of Toronto, Toronto, Ontario, Canada*
[2]*Department of Biomedical Engineering, University of Virginia, Charlottesville, VA 22908, USA*

Over the past decade, non-invasive preclinical imaging has emerged as an important tool to facilitate biomedical discovery. Not only have the markets for these tools accelerated, but the numbers of peer-reviewed papers in which imaging end points and biomarkers have been used have grown dramatically. High frequency 'micro-ultrasound' has steadily evolved in the post-genomic era as a rapid, comparatively inexpensive imaging tool for studying normal development and models of human disease in small animals. One of the fundamental barriers to this development was the technological hurdle associated with high-frequency array transducers. Recently, new approaches have enabled the upper limits of linear and phased arrays to be pushed from about 20 to over 50 MHz enabling a broad range of new applications. The innovations leading to the new transducer technology and scanner architecture are reviewed. Applications of preclinical micro-ultrasound are explored for developmental biology, cancer, and cardiovascular disease. With respect to the future, the latest developments in high-frequency ultrasound imaging are described.

Keywords: micro-ultrasound; angiogenesis; mouse imaging; phenotyping; cancer models; cardiovascular disease

1. INTRODUCTION

Modern biomedical research is rapidly evolving to include sophisticated imaging analysis using optical, magnetic resonance, computed tomographic and nuclear imaging technologies. Over the past decade these modalities have been re-engineered to specifically address the needs of researchers seeking to analyse living animals in longitudinal studies of disease models and normal development. The genomics revolution, with its concomitant proliferation of disease models and genetic mutants, has put a strong focus on the mouse. Each of the modalities has therefore struggled to scale imaging performance and resolution to work effectively in small animals. The effect of these developments has been to create a new and rather large market for preclinical imaging that was estimated to be over about $500 million in 2010. Ultrasound, by virtue of its high resolution, rapid frame rate, and low cost has emerged a strong competitor in this field with approximately 13 per cent of the installed preclinical imaging base in 2010 [1].

*Author for correspondence (stuart.foster@sunnybrook.ca).

One contribution of 15 to a Theme Issue 'Recent advances in biomedical ultrasonic imaging techniques'.

The technological evolution of high-frequency micro-ultrasound traces its roots back to the late 1980s when Sherar *et al.* [2] first demonstrated non-invasive imaging of tumour spheroids at 100 MHz. Success in simple biological systems quickly focused attention on potential clinical applications. Independently, pioneering researchers converged on three important clinical applications of high-frequency B-mode imaging: ophthalmology [3–5], dermatology [6,7] and intravascular ultrasound [8–10]. In 1995, Turnbull *et al.* [11] published a paper on the use of high-frequency ultrasound to phenotype living mouse embryos and essentially ushered in the modern era of preclinical imaging with ultrasound. Since that time, systems and applications have proliferated in a wide range of areas including cardiovascular research, cancer, developmental biology and many others. The ultrasonic visualization of living tissue at microscopic resolution is referred to in the clinical literature as 'ultrasound biomicroscopy' (UBM). In the field of preclinical imaging it is often referred to as 'micro-ultrasound' by analogy to the other preclinical imaging modalities such as micro-positron emission tomography and micro-computed tomography. A review of the early history of micro-ultrasound is given by Foster *et al.* [12].

This paper describes the technological evolution of micro-ultrasound and some of the latest applications

Received 5 April 2011
Accepted 13 May 2011

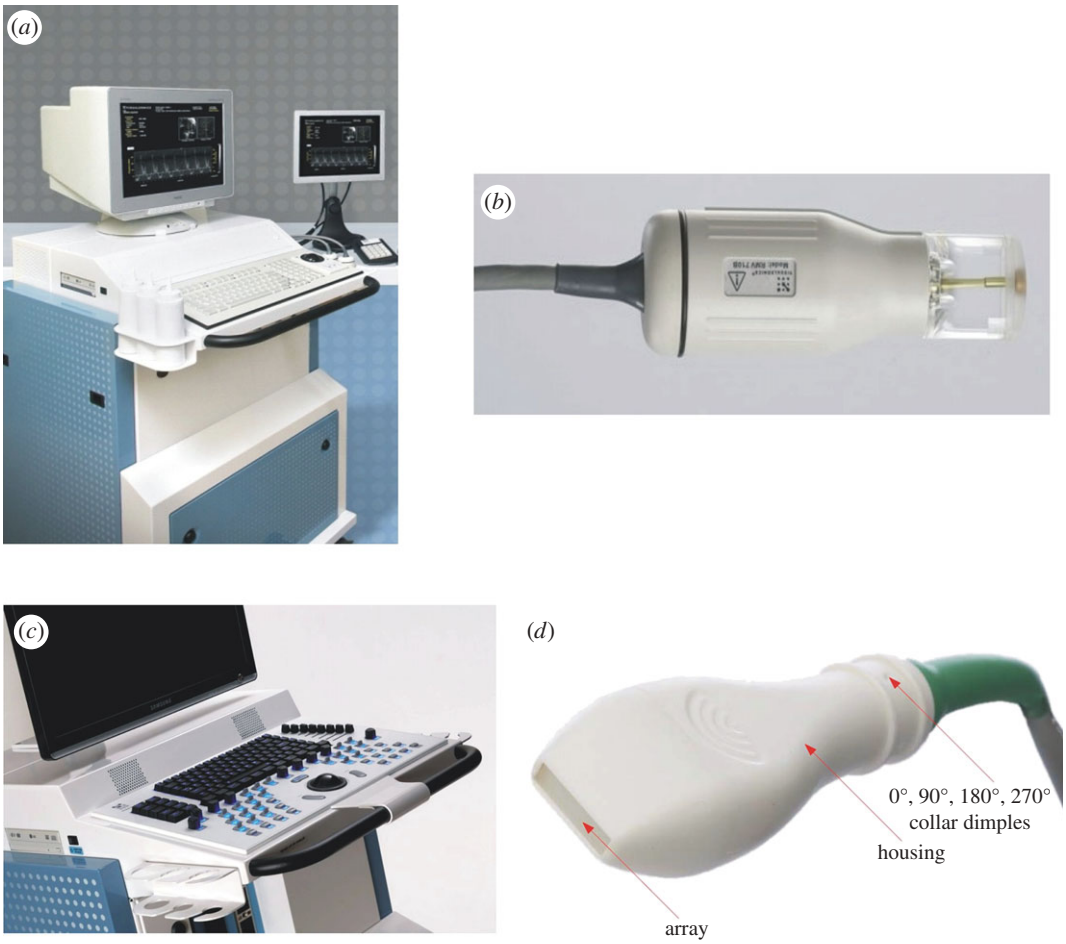

Figure 1. High-frequency micro-ultrasound imaging systems developed over the past 10 years have enabled efficient, high resolution, quantitative analysis of animal models of disease. Earlier systems (*a*) relied on mechanically steered single element scanheads (*b*). More recently, fully beam-formed scanners (*c*) have been developed using novel high-frequency arrays (*d*). The latter devices use no mechanical actuation and improve the depth of field of the imaging system.

in biomedical research. Well-established B-mode, Doppler and contrast imaging approaches for micro-imaging are reviewed and their limitations discussed. These methods are discussed in the context of applications in three sections devoted to developmental biology, cancer and cardiovascular disease, respectively. The use of microbubble (MB) contrast agents with both linear and nonlinear imaging sequences are examined as a means of functional imaging of the microcirculation. Targeted MB contrast for molecular imaging is also explored and the development of parametric imaging is described. The strengths and weaknesses of these new methods are discussed and the potential for their use in preclinical animal drug studies, and novel therapeutic studies is described.

2. INSTRUMENTATION

The general design considerations for high-frequency ultrasound imaging derive from the trade-offs between frequency, penetration and resolution. Not surprisingly, these factors cannot be considered independently but must be approached through a series of compromises as outlined by many authors (see [12,13]). The frequency-dependent attenuation of ultrasound limits the total ultrasound path in tissue to about 600 wavelengths round trip or a maximum depth of 300 wavelengths. Based on this criterion, imaging 10–30 mm of mouse tissue suggests minimum wavelengths of 33 μm (45 MHz) to 100 μm (15 MHz), respectively. Diffraction dictates that resolution in ultrasound is proportional to the product of the wavelength and the *f*-number (focal length/aperture diameter) of the beam. Thus an *f*/2 beam at 30 MHz will have a lateral resolution of approximately 100 μm and at 15 MHz, 200 μm. This is ideal for imaging of mice and rats and creates a level of scaled resolution similar to what is observed when using clinical ultrasound on humans.

Based on the success of early prototype systems, preclinical micro-ultrasound was commercialized [14] to meet the growing demand for imaging tools in the biological community (figure 1*a*). Significant progress was made with mechanically scanned single element transducers such as the one shown in figure 1*b*. This scanhead contains the high-frequency transducer in a sealed liquid-filled compartment that is coupled to the mouse skin using an ultrasound gel. Remarkably, these probes were capable of reaching frame rates in excess of 100 Hz. Several hundred peer-reviewed papers using the single element scanned micro-ultrasound platform have now been published. Overviews related to applications of micro-ultrasound in

developmental biology are available (e.g. [15–19]). In the area of cardiovascular research see, for example [20–23], and in the area of cancer see, for example [24–28]. While single element systems have fared well in the market they suffer from serious limitations in depth of field, in their ability to provide functional maps of Doppler blood flow in real time, and in their ability to image contrast agents. In 2009, systems based on linear transducer array technology were finally introduced to solve these problems [29]. The new imaging technology was commercialized by VisualSonics and enables the frequency of systems based on linear transducer arrays to be extended from 15 to above 50 MHz. Photographs of the linear array instrument and scanhead that currently defines the field of micro-ultrasound imaging are shown in figure 1*c*,*d*. It is expected that the technology will continue to evolve towards two-dimensional arrays via the exploitation of capacitive micro-machined devices but this is probably years into the future.

2.1. Imaging protocols

Animals studied under approved protocols are positioned on an imaging platform that presents the region to be imaged to a scanhead rigidly attached to a mechanical positioning system as shown in figure 2*a*. This allows hands-free positioning and capture of the images. The animal is first anaesthetized using a 2 per cent isoflurane mixture in oxygen or air and hair (if present) is removed using a depilatory cream. Injectable anaesthetics are often used as well. The mouse is then restrained on the heated imaging platform with surgical tape to maintain normal body temperature of the animal during imaging. A warmed ultrasonic gel is applied to the mouse's skin to couple the scanhead before imaging. Key physiological parameters are captured from the platform including heart rate, temperature, respiration and electrocardiogram. These signals are gathered through paw and temperature probes and integrated with the real-time micro-ultrasound images.

A typical imaging configuration is illustrated in figure 2*a* in which the system operator has a mouse on the imaging platform with required instrumentation. A flexible but lockable arm holds the transducer adjacent to the tissue to be imaged. Some users who are experienced sonographers prefer to scan with the transducer hand held, as they would in a clinical exam, because they feel it gives them more direct control over the orientation of the scan plane. In the background, the anaesthesia delivery, induction chamber and monitoring equipment is shown on the right. Images such as the one shown in figure 2*b* show the results of an upper abdominal image of an adult mouse. The depiction of organs and other vascular structures is remarkably similar to human images made at much lower frequencies. Visible are the overlying liver, the right kidney, adrenal gland, vena cava, aorta and portal vein. An additional accessory to the imaging platform is an injection mount that allows for the guidance of precise injections or biopsies *in vivo* through the real-time imaging guidance of the micro-ultrasound system.

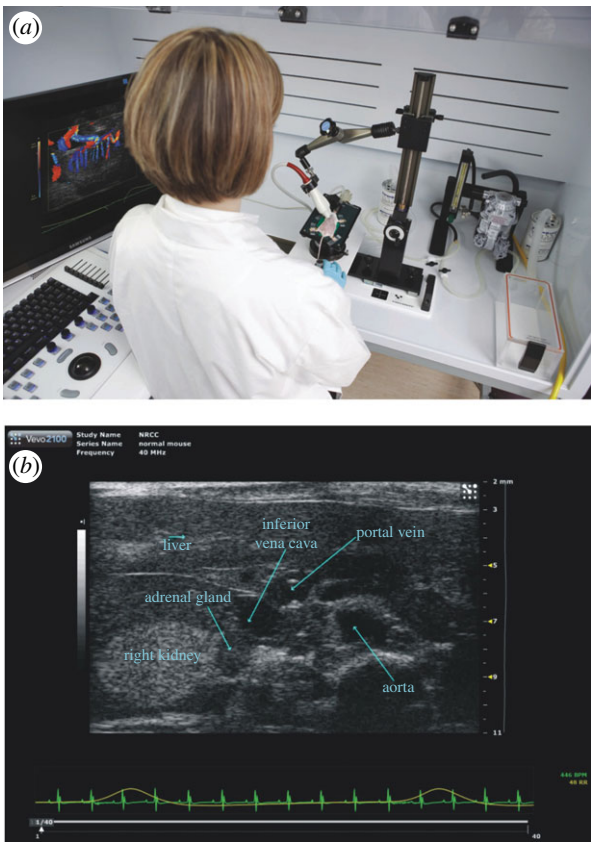

Figure 2. (*a*) The imaging system of figure 1*c* being used to image a mouse. The mouse is anaesthetized and lying on a heated stage and is monitored for heart rate, breathing, and in some cases blood pressure. Scanning is performed after removal of hair (if necessary) and after the application of a heated gel to the region of interest. The ultrasound scanhead is mounted on a 'Rail System' inside a biosafety cabinet to reduce jitter in the image due to hand motion. (*b*) Example of a still frame from a real-time sequence of images of the abdominal region of the mouse. This 'B-scan' image shows, from left to right, a section through the kidney, adrenal gland, the vena cava, portal vein, and the aorta.

For ultrasound contrast and targeted imaging studies (described in detail in the next section), MB agents such as MicroMarker (VisualSonics, Toronto) or Definity (Lantheus, Montreal) can be reconstituted according to manufacturers' specifications and injected via tail vein in volumes that typically do not exceed 100 µl. For targeted imaging studies, streptavidin-coated MicroMarker agents are used. Once reconstituted, targeting ligands are attached to the coated MBs using biotin–streptavidin coupling chemistry to optimally saturate MB surface with antibodies while minimizing non-conjugated antibodies in the solution. Targeted MBs are typically functionalized with biotinylated rat anti-mouse monoclonal antibodies such as vascular endothelial growth factor receptor 2 (VEGFR-2; Avas12a1, eBiosciences, San Diego, CA, USA) and are injected into the tail vein with a 25 G needle.

2.2. Microbubble contrast imaging

Ultrasound contrast agents, comprised of gas bubbles less than 5 µm in diameter and encapsulated by a

polymer or lipid shell, represent a special kind of scattering source that is critical to the development of molecular imaging with ultrasound. Details of the chemistry and fabrication of targeted MBs are described by Borden *et al.* [30]. Whereas nonlinear propagation of ultrasound results in the creation of harmonics, scatter from MBs is governed by somewhat more complex interactions that result in the creation of other spectral features unique to MBs. The radial motion of the wall of an MB under insonation is most often described by the Rayleigh–Plesset equation [31]. It is a fortunate coincidence of nature that insonation in the MHz frequency range excites bubble resonance due to the compressible nature of the gas inside the bubble. The frequency of MB resonance is a function of the gas properties and the shear modulus of the MB shell. Resonance leads to a very strong backscattered contrast signal often visible above the scatter from other tissue structures. By subtracting pre- from post-contrast images it is possible to show specific regions of contrast enhancement. This is the basis of contrast imaging in the mechanically scanned micro-ultrasound systems. More powerful means of enhancing contrast while suppressing tissue are based on nonlinear interactions. With increased incident amplitudes, the bubbles can be driven to oscillate nonlinearly resulting in the scattering of energy to harmonic multiples of the transmit frequency (f_o) and to non-integer multiples of the fundamental such as $1/2f_o$, $3/2f_o$, $5/2f_o$, etc. The component at half the fundamental is referred to as the subharmonic, while the other non-integer harmonics are referred to as ultraharmonics. The challenge of MB contrast imaging has been to develop specific pulse sequences and signal processing that maximizes detection efficiency for signals arising from MBs while suppressing signals arising from tissue or nonlinear propagation. This has generally required the development of pulse sequences in which the phase and amplitude of the insonifying pulse are manipulated to suppress or enhance particular linear and nonlinear components. One approach known as 'pulse inversion imaging' was developed by Hope-Simpson *et al.* [32] and is now a standard method implemented on clinical instruments. Techniques such as harmonic imaging [33] and pulse inversion [32] exploit the second harmonic ($2f_o$) to provide greater contrast with respect to the surrounding tissue. Burns & Hope-Simpson [34] patented the concept of combining phase and amplitude processing for optimized nonlinear contrast imaging and Doppler. This idea was further refined by Haider & Chiao [35] and evolved into commercially available contrast pulse sequences. Eckersley *et al.* [36] showed that phase and amplitude modulation (PIAM) applied together provided 14–18 dB enhancement of contrast signals over linear scatterers for insonifying pulses having a centre frequency of 2.5 MHz. The detection of energy in the subharmonic and ultraharmonic frequency range has also been explored by a number of investigators [37–41] and is of particular interest because these signals arise only from MB interactions. At diagnostic frequencies, PIAM processing retains an advantage over subharmonic imaging in that resolution is not compromised.

The above methods for contrast imaging are well established for low MHz clinical imaging and have been recently evaluated and implemented for high-frequency micro-ultrasound as described by Needles *et al.* [42]. Based on the phantom characterization, AM/PIAM contrast processing was recently demonstrated to provide a contrast to tissue ratio (CTR) improvement of 13 dB at 20 MHz but there is evidence that CTR diminishes with increasing frequency. Greater than 10 dB suppression was observed at a frequency of 24 MHz [42]. The use of these approaches remains problematic and additional research is needed to improve high-frequency performance.

3. APPLICATIONS: DEVELOPMENTAL BIOLOGY

Micro-ultrasound is an important imaging modality for studies in developmental biology. It is useful for assessing maternal, placental and foetal haemodynamics and morphology and growth, as well as for image-guided *in utero* interventions, and teratology (e.g. [43]). It has proven utility in studies examining normal development, as well as abnormal development in genetically altered mouse models. By design, the ultrasound frequency, imaging window size, and depth of resolution have been optimized for mice because of the prominent and growing role of this species in developmental research. The relatively small depth of penetration achieved at 40 MHz (approx. 1 cm) means that micro-ultrasound is less well suited to examination of developing embryos in larger species. However, it can be used to study cardiovascular function in developing chick embryos studied *ex ovo* [44].

The advent of micro-ultrasound has propelled the use of mouse models in translational research relevant to obstetrics. Micro-ultrasound generates images and Doppler recordings of the conceptus in mouse pregnancy that rival those obtained in humans with clinical ultrasound instrumentation despite the vast differences in size. One notable difference in the appearance of cardiovascular images of mouse embryos versus human foetuses is the echogenicity of blood. Throughout most of gestation, human foetal blood is relatively anechogenic so blood spaces appear dark. However, the echogenicity of mouse embryo blood increases with frequency and is relatively high as a result of the nucleation of red blood cells at this stage with a peak echogenicity at E13.5 [45]. This reduces blood–tissue contrast in images of mouse embryos. Echogenicity of embryonic blood decreases in late gestation as red blood cells lose their nuclei.

3.1. Evaluation of embryonic development during pregnancy

An important application for micro-ultrasound is the evaluation of embryonic development during pregnancy. It has been used to determine the timing and extent of embryonic lethality non-invasively, and for quantifying the rate of growth of the conceptus, the embryo, the placenta, and specific organs within the conceptus including the developing eye [18,46,47]. Given the high reproducibility of morphological development and growth of normal embryos, and the

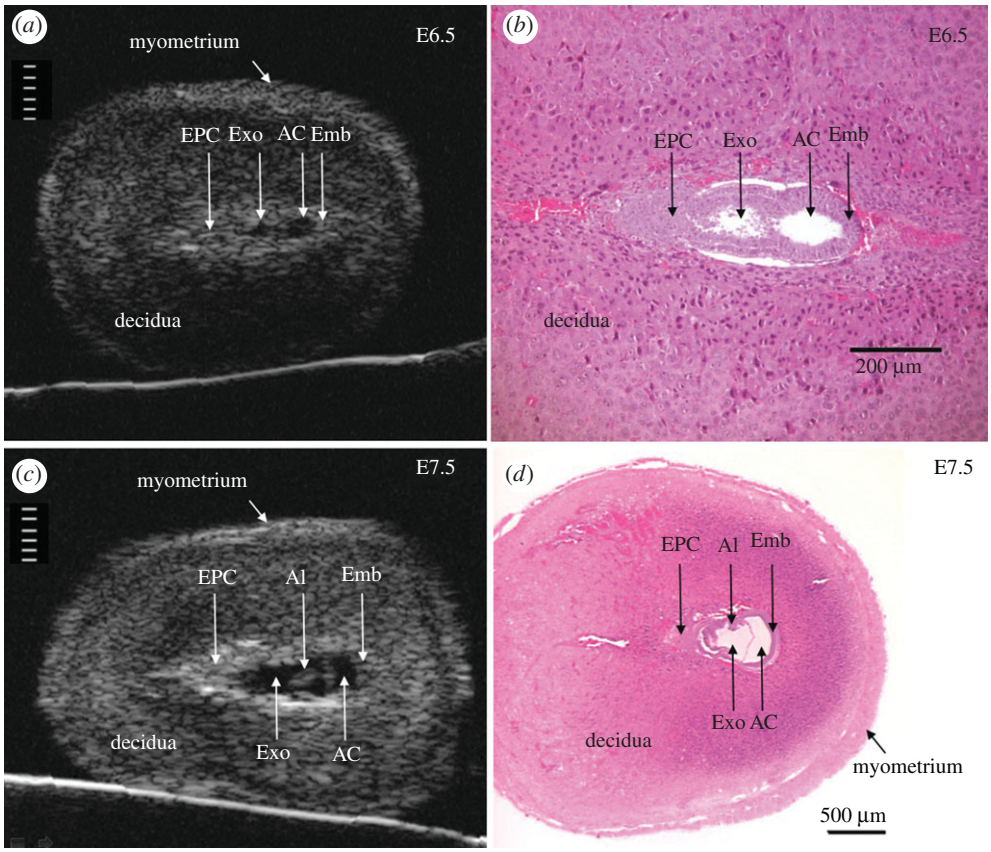

Figure 3. Anatomical detail visible in ultrasound images of the conceptus in the exteriorized uterus at E6.5 and E7.5. Ultrasound images (*a*,*c*) and H and E histological sections (*b*,*d*) of implantation sites at E6.5 (*a*,*b*) and E7.5 (*c*,*d*). Divisions in the scales in (*a*) and (*c*) are 100 µm apart. The conceptus in histological sections is smaller than *in vivo* due to shrinkage during tissue preparation (fixation and dehydration). AC, amniotic cavity; Al, allantois; Emb, embryo; EPC, ectoplacental cone region; Exo, exocoelomic cavity. Adapted from [48].

high resolution of micro-ultrasound, micro-ultrasound measurements can be used in normal pregnancies for gestational staging [47]. Equations predicting gestational age or embryonic weight from ultrasound measurements are available [47].

The amount of detailed phenotypic information that can be obtained from the conceptus using micro-ultrasound increases as gestation advances [16,19,47,48]. At E6.5 (approx. 2 days after implantation), the implantation site is often sufficiently clearly visualized to enable the size of the conceptus to be quantified (figure 3) [16,48]. By E7.5, conceptus size can be routinely obtained [47] and other structures such as the allantois and amnion are visible (figure 3) [16,48].

The onset of cardiac function can be detected when it occurs at approximately E8.5 [16,49,50]. At this stage, it becomes possible to use Doppler to measure heart rate, to detect arrhythmias and to use electronic callipers to measure cardiac size in addition to the size of the embryo and conceptus. Vitelline blood flow to the yolk sac also becomes detectable at this stage [51]. By E9.5, blood flow through the umbilical artery to the placenta begins and Doppler arterial waveforms can be obtained [51,52]. Also by E9.5, images of the heart can be used to position Doppler sample volumes to record ventricular inflow and outflow waveforms as shown in figure 4 [16]. At this stage, the heart is a U-shaped tube. Imaging and Doppler assessment is possible at E10.5–E12.5 but is easier later in gestation (≥E13.5) when the heart is larger (figure 4). By E13.5, four cardiac chambers are visible although septation is not fully complete. At this stage, heart examinations similar to those performed routinely in adult hearts can be performed when embryos are in a suitable orientation to obtain the required cardiac view [50]. Micro-ultrasound has been used to study normal cardiac function during embryonic development [50,53,54]. In addition, the embryo can be visualized in three dimensions *in utero* as shown in figure 5. The development of other embryonic structures can be examined including the eye, brain, paws, lungs and liver [47,54].

3.2. Morphology of the developing embryonic eye

The eye has particularly high tissue contrast and its growth during embryonic development has been studied in detail (figure 6) [46]. The very earliest visualization of ocular development using non-invasive imaging is at about E9.5 where the micro-ultrasound image shows a small invagination of the optic placode in the forebrain and E10.5 images show the optic vesicle as an echolucent sphere with a diameter of approximately 250 µm [46]. Between E10 and E11, the lens placode first creates the lens pit and ultimately the lens vesicle. At E11.5, the lens vesicle has developed and appears as a spherical cavity with an echogenic border

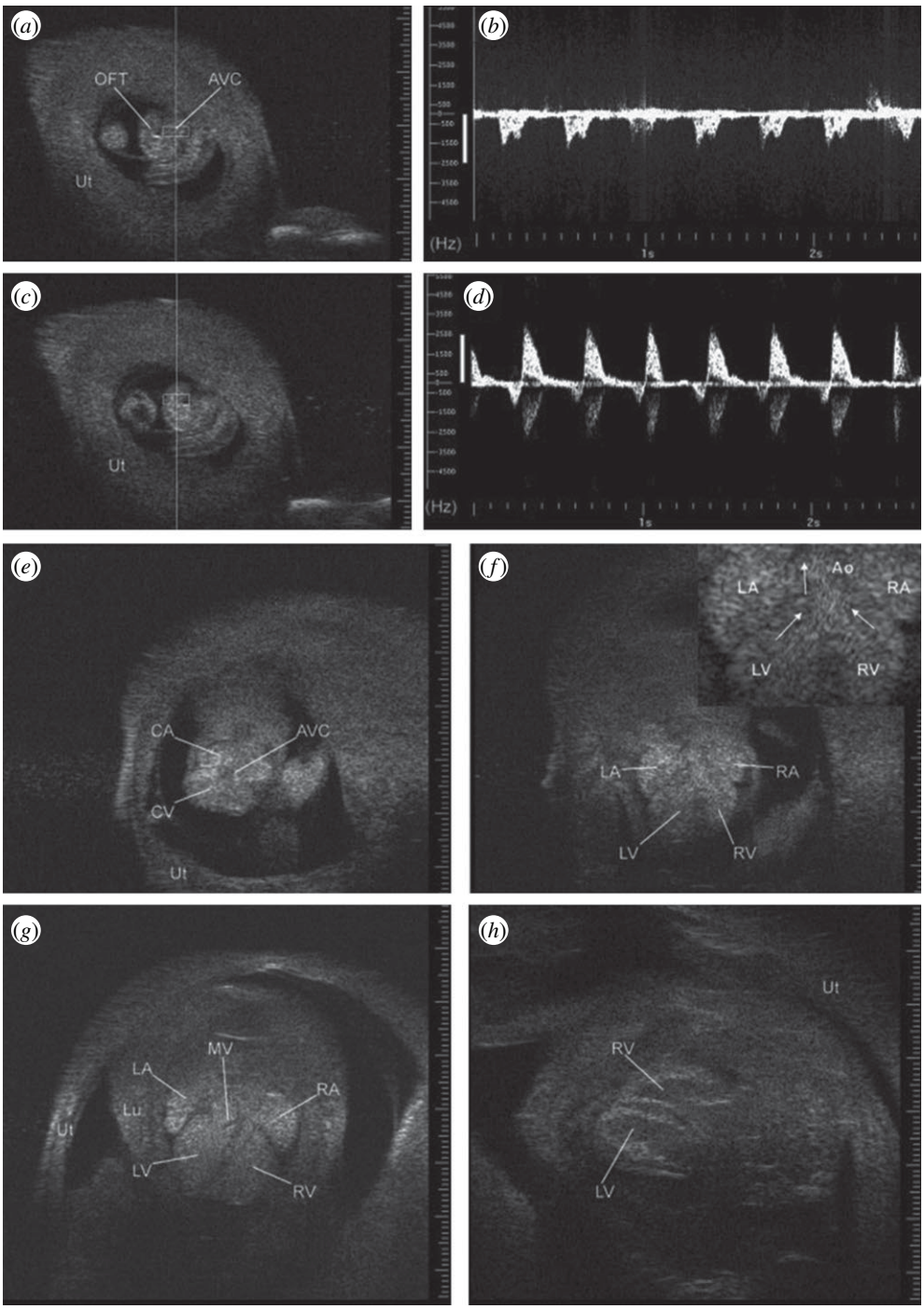

Figure 4. Images of the embryonic heart as it develops from a U-shaped tube at E9.5 to a four-chambered structure at E16.5 when viewed through the exteriorized uterus (Ut) using 55 MHz. (*a*) U-shaped embryonic heart at E9.5. Doppler sample volume (rectangle) within atrioventricular canal (AVC) generated ventricular inflow Doppler waveform in (*b*). (*c*) Doppler sample volume in the outflow tract (OFT) generated the Doppler waveform in (*d*). (*e*) Transverse view at E10.5 showing common atrium (CA), common ventricle (CV), and common atrioventricular canal (AVC). (*f*) Transverse view at E12.5 showing left and right atrium (LA, RA) and left and right ventricle (LV, RV) with enlargement in inset with arrows highlighting streamlines towards the aorta (Ao). (*g*) Transverse view at E13.5 with mitral valve leaflets (MV) and complete septum visible (Lu, lung). (*h*) Long-axis view of ventricles at E16.5. Echogenicity of embryonic blood tends to reduce blood–tissue contrast but this effect attenuates near term. Adapted from [22].

circumscribed by a narrow hypoechoic rim (figure 6, arrow). Evidence of retinal development is seen at E13.5, and the posterior aspect of the lens vesicle exhibits a thickening of its echogenic border. Evidence of corneal development is seen at E14.5. At E14.5, the micro-ultrasound image shows the posterior segment of the lens vesicle splitting into three distinct layers: the developing vitreous cavity (anechoic), immediately posterior to the lens followed by the retina (echoic), and the intraretinal space (anechoic). Micro-ultrasound images of the primary ocular tissues from E14.5 to E18.5 demonstrate progressive morphogenesis of the

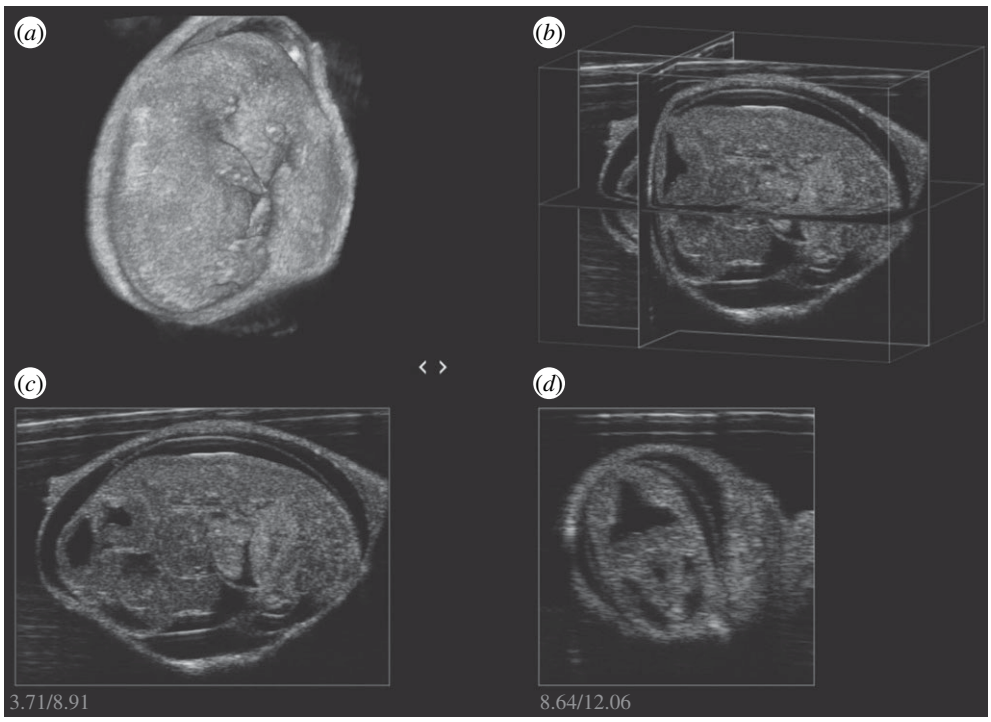

Figure 5. (*a*) Mouse embryo at E13.5 imaged in three dimensions in an exteriorized uterus using an MS550 linear array (VisualSonics, Toronto). Intersecting planes can be displayed in arbitrary directions (*b*) or as separate planes (*c*,*d*).

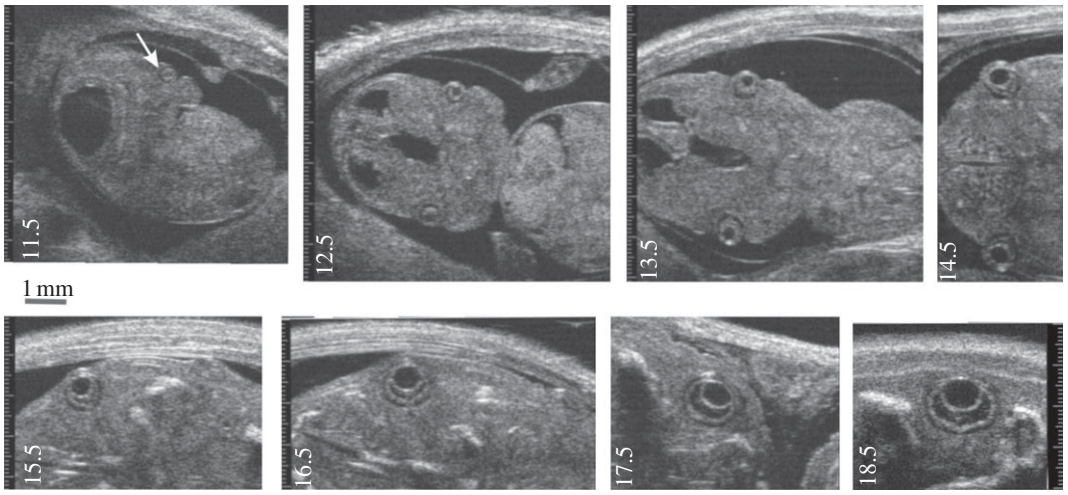

Figure 6. Representative images of ocular development in the mouse. Visible structures include the optic placode and vesicle (arrow) at E11.5, evidence of retinal development at E13.5, corneal development at E14.5 and progressive morphogenesis of the eye between E15.5 and E18.5. Adapted from [46].

eye as shown in figure 6. The development of the lid and iris was difficult to visualize with micro-ultrasound, as their echogenicity appeared to be similar to that of surrounding tissue. Additional detail on the embryonic development process for the eye is given in [46].

3.3. Evaluation of the role of the mother and placenta in embryonic development

The development of the embryo is dependent on appropriate adaptations in maternal physiology to support the pregnancy and on the function of the placenta. There are large changes in maternal cardiovascular function during pregnancy in mice, as in other animals [55,56]. Micro-ultrasound studies have shown that maternal cardiac output increases, the cardiovascular system enlarges and uterine arterial blood flow increases to meet the perfusion requirements of the rapidly growing conceptuses during pregnancy [51,55]. In addition, micro-ultrasound enables visualization (figure 7) of the spiral arteries that form within the maternal decidua at embryonic implantation sites, and of the trophoblast canals that form within the placenta to deliver maternal blood to the placental exchange region known as the labyrinth in mice [57]. These changes are required to ensure adequate perfusion of maternal blood through the labyrinth to support gas, nutrient and waste exchange with the embryo. The

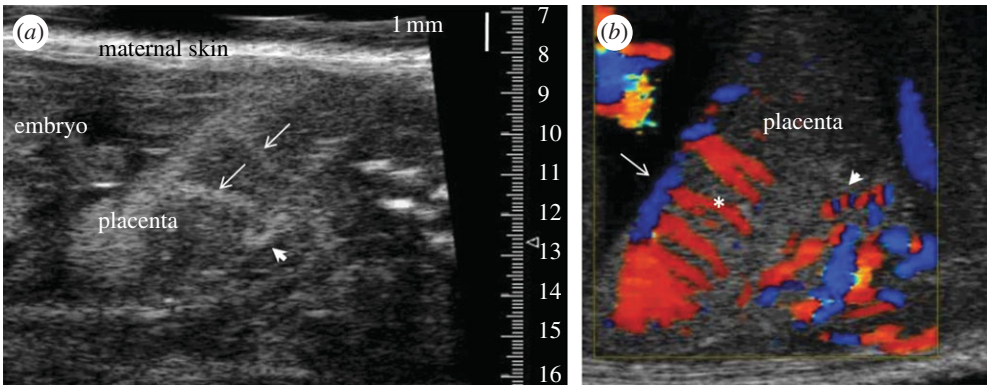

Figure 7. Micro-ultrasound imaging of the placental circulation in the mouse. (*a*) Contrast enhanced visualization of the uteroplacental blood supply to the mouse placenta using MBs infused into the maternal circulation at E14.5. A spiral artery in the decidua is indicated by the arrowhead. Arrows show the maternal arterial canals. Canals are formed by foetal trophoblast cells and they direct maternal blood from the spiral arteries into the labyrinth, the exchange region of the placenta. (*b*) Colour Doppler imaging of the uteroplacental and foetoplacental blood supply to the mouse placenta at E14.5. A spiral artery is shown by the arrowhead. The spiral movement of blood in the maternal spiral artery causes the red–blue alternating pattern as the blood alternates between flowing towards and away from the transducer. Flow in the foetal chorionic plate vessels (arrow) and in the foetoplacental arterioles (asterisk) directs foetal blood deep into the labyrinth exchange region of the placenta.

importance of considering maternal influences on embryo development and survival is highlighted by a recent study using micro-ultrasound to serially evaluate embryonic viability in mothers from 39 interspecific recombinant congenic strains. Congenic mothers were bred to wild-type fathers in this study. Three quantitative trait loci for maternal traits responsible for embryonic lethality were found [58]. Thus, micro-ultrasound in developmental biology research facilitates incorporation of maternal function and its effects on development and viability of the conceptus.

The placenta is also critically required for normal development of the embryo. Micro-ultrasound has been used to visualize and to record Doppler blood velocities in the uteroplacental circulation including the uterine artery, spiral arteries and maternal arterial canals in the placenta as shown in figure 7 [51]. Increases in the velocity of maternal blood flow at these sites have been quantified throughout gestation [51]. Further image enhancement using colour Doppler imaging facilitates detection of the uterine artery in the maternal abdominal cavity, and of the maternal spiral arteries in the decidua (figure 7). MB contrast agents (see §2.2) administered into the maternal circulation can also be used to highlight maternal blood flow through the uteroplacental circulation (figure 7). Micro-ultrasound has been used to visualize and record Doppler blood velocities in the developing placental circulation of the conceptus including the vitelline vessels to the yolk sac, the umbilical vessels, as well as the chorionic and foetal arterioles within the placenta itself (figure 7) [51,52]. Colour Doppler imaging can also be used to enhance visualization of these vessels as demonstrated in figure 7.

3.4. Evaluation of embryonic and postnatal cardiovascular development and function

The widest application of micro-ultrasound in developmental biology has been for the evaluation of cardiovascular development and function. Doppler waveforms can readily be obtained from the heart and other sites in the foetal circulation including the ascending and descending aorta, pulmonary arteries, ductus arteriosus, ductus venosus, inferior vena cava, and cerebral and placental vasculatures. Micro-ultrasound has proved valuable for *in vivo* phenotyping of defects in cardiovascular function in embryos and during postnatal development caused by genetic alterations. Examples include evaluations of cardiac function in embryos with mutations in Fgl2, NFATc1, BMPRIA or Baf60c [50,59–61]. Important cardiovascular events occur at birth when the placenta is lost from the circulation and a large increase in pulmonary blood flow occurs. This switch enables the lungs to provide gas exchange after birth. Events include closure of the ductus arteriosus, a short but large diameter shunt that connects the pulmonary trunk to the descending aorta in embryonic life. In mice, closure normally occurs within hours of birth [62]. Micro-ultrasound colour Doppler imaging can be used to visualize the early postnatal ductus arteriosus in neonates on the day of birth as shown in figure 8. Colour Doppler imaging that is now possible in the new linear arrays greatly facilitates placement of the Doppler sample volume within the ductus (figure 8). Progress in postnatal closure of the ductus arteriosus can be inferred from Doppler blood velocity waveforms obtained at this site (figure 8). Further developmental changes in cardiac function occur in the weeks following birth and these can be monitored by micro-ultrasound (e.g. [50,53,54]).

A growing area of research in developmental biology investigates how the early environment of the embryo and neonate influences long-term cardiovascular outcomes in adulthood (e.g. [63]). The ability to use micro-ultrasound as a consistent technology to perform serial examinations throughout development from the embryo to the adult facilitates such research by avoiding errors due to changes in technology, and by reducing the number of animals required for study. Serial examinations have been used to investigate cardiovascular changes during normal development and alterations caused by genetic mutation (e.g.

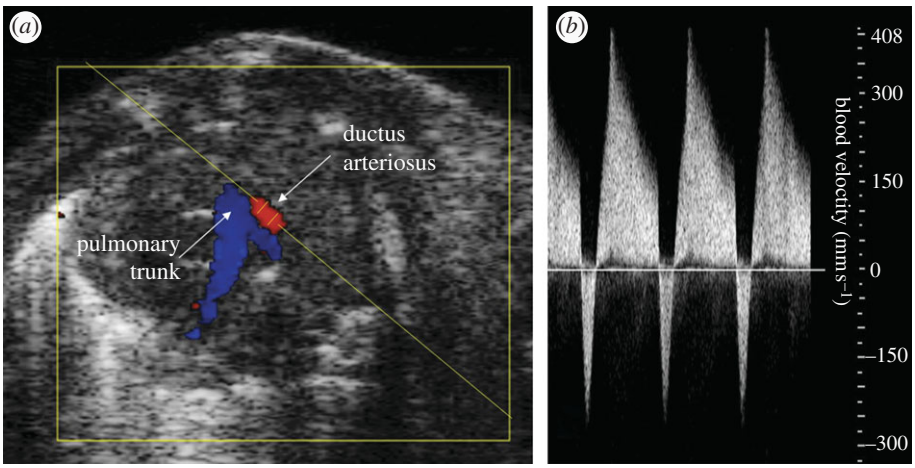

Figure 8. Colour Doppler image showing the pulmonary trunk and ductus arteriosus of a mouse neonate within hours of birth before closure of the ductus arteriosus. (*a*) Blood flow in the pulmonary trunk is away from the transducer (blue) and flow in the ductus arteriosus is towards the transducer (red). The angled yellow line shows the angle of insonation and the gap in the yellow line within the ductus arteriosus shows the position of the Doppler sample volume. (*b*) The ductus arteriosus is still open so the Doppler blood velocity waveform shows prominent flow towards the pulmonary trunk through the ductus arteriosus (positive velocity) in systole and brief flow reversals towards the aorta (negative velocity) in diastole.

[50,53,54]). However, the bioeffects of micro-ultrasound on mouse embryonic development and on long-term outcomes are not well understood. Modest bioeffects of diagnostic levels of ultrasound caused by a single imaging session have been reported; small transient reductions in postnatal body weight have been observed [64,65] as have subtle changes in adult neurobehaviour [66]. Isoflurane anaesthesia is often used for immobilization during imaging, and it may also have developmental effects [67]. Minimal effects of repeated ultrasound examinations under isoflurane anaesthesia on newborn mouse growth and cardiac diastolic function were observed previously [54]. Nevertheless, in studies of developmental biology, limiting the duration and number of ultrasound examinations and incorporating sham controls into study designs are recommended.

3.5. Ultrasound guidance for prenatal interventions

Micro-ultrasound has proved to be useful as a tool for targeting interventions to specific sites within the conceptus. The embryonic brain has been a common target. These studies and the methods involved have recently been reviewed [17]. Image-guided microinjection has also been used to target the early placenta as shown in figure 9 [48] in which a microinjection catheter is shown with its tip in the exocoelomic cavity of an E17.5 embryo. Other targets for guided injection include the embryonic heart [68], developing skin [69], spine, and eye [70]. These injections are primarily to deliver viral constructs to influence gene expression, genetic material or therapeutic payloads. Figure 10 shows an excellent example of a guided injection into the spinal canal of an E14.5 embryo. Progressive penetration to the target illustrates dramatically the importance of imaging feedback in this highly compliant tissue.

4. APPLICATIONS: CANCER

In the past decade, new targeted therapeutics have shown clinical benefit in patients with metastatic colorectal cancer, advanced non-small cell lung cancer, hepatocellular carcinoma, metastatic breast cancer, renal cell carcinoma and other cancers [71–75]. However, the results of these therapies have been modest in terms of survival benefit and the cracks in our understanding of how these drugs work—and sometimes fail to work—are now evident. Most prominent are the lack of understanding of the mechanisms of action of the drugs, the inability to identify which patients might ultimately benefit from treatment, the lack of effective biomarkers to predict and track treatment response and, most significantly, the development of resistance to therapy. Currently, the putative mechanisms of action are quite controversial and clearly depend on the type of drug, the targeted pathways, the nature of the agent (e.g. small molecule versus antibody) and the range of drug specificity ('promiscuity'). Micro-ultrasound is well suited to probing some of these questions in preclinical models. It is an imaging modality that can be used to visualize, characterize and quantify orthotopic and subcutaneous xenografts, and spontaneous tumours in mice and rats. Tumours can be monitored and quantified from initiation through their growth stages and on to metastases in distal organs, lymph nodes and other tissues. The current imaging systems (figure 1*c*,*d*) allow real-time visualization and measurement of the tumours in two and three dimensions. Three-dimensional imaging is accomplished by attaching the probe to an automated stage available as an accessory on the scanner. Blood flow, vascular architecture and assessment of feeder vessels can be quantified using power Doppler (for vessels larger than 30 μm) and tumour perfusion and micro-circulatory flow can be assessed using contrast agents *in vivo*. The latter is particularly important in studies of antiangiogenic therapeutics.

4.1. Tumour sizing and quantification in two and three dimensions

One of the most important measurements in oncology is quantifying the change in tumour volume during

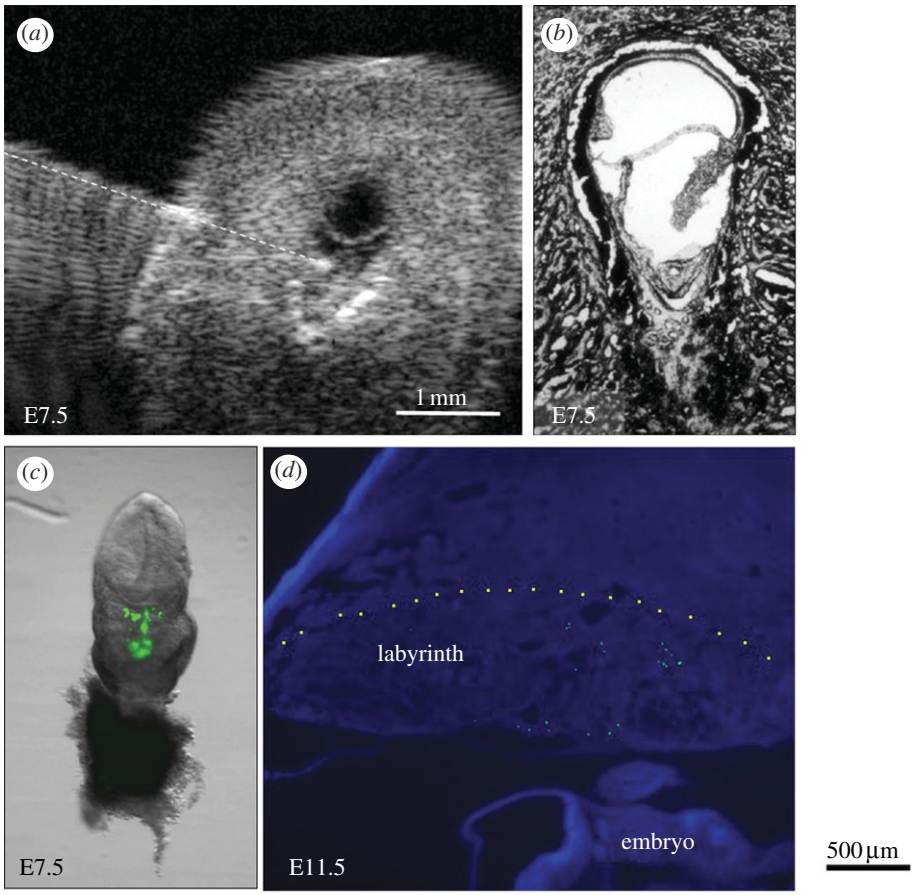

Figure 9. Ultrasound-guided microinjection of green fluorescent microspheres into the exocoelomic cavity of a mouse conceptus at E7.5. (*a*) The glass microinjection catheter (highlighted with a dashed line) is shown with its tip in the exocoelomic cavity in an exteriorized conceptus. (*b*) Histological image showing the anatomy of the conceptus at E7.5. (*c*) A conceptus dissected on the day of injection showing green fluorescent microspheres in the exocoelomic cavity. The embryo will form above and the placenta below this cavity. (*d*) A placenta dissected later in gestation at E11.5 showing green fluorescent microspheres confined within the labyrinth region of the placenta. Adapted from [48].

disease progression and changes related to tumour response to anti-cancer therapy [76–78]. Because micro-ultrasound is non-invasive, tumour growth and changes can be monitored repeatedly and longitudinally in the same animal, which can serve as its own control, thereby increasing the accuracy of the experiment and reducing the number of cohort animals required. Cheung *et al.* [79] originally described the use of micro-ultrasound in the assessment of xenograft growth analysis. It is now routinely used in serial two-dimensional and three-dimensional volumetric quantification of tumour sizing *in vivo* in a variety of rodent and non-rodent cancer models [25,26,80–85]. Micro-ultrasound has been shown to more accurately track tumour volume than external callipers [86]. Wirtzfeld *et al.* [77] described the use of micro-ultrasound to track three-dimensional tumour volumes in progression in a transgenic prostate cancer mouse model. Three-dimensional micro-ultrasound images correlated closely to serial histology (a correlation coefficient of 0.998 ($p < 0.001$)). Furthermore, three-dimensional micro-ultrasound measurements accurately confirmed the size and shape of these tumour masses *in vivo* [77]. The technique is highly reproducible as tumour detection sensitivity and specificity were both more than 90 per cent when diagnoses were based on repeated micro-ultrasound examinations performed on separate days. Further studies went on to show the utility of three-dimensional micro-ultrasound to not only non-invasively track the growth of liver metastases (tumour diameter, volume and growth curve), but also to evaluate potential chemotherapeutics on these parameters in a longitudinal murine metastases model [26].

4.2. Evaluation and quantification of tumour blood flow

Aberrant microcirculatory morphology and haemodynamics are signatures of human diseases such as cancer, macular degeneration, diabetes, psoriasis and many others. The need for non-invasive means to visualize these processes in biomedical research and clinical practice is compelling. In preclinical research, detailed knowledge of microvascular patterning and haemodynamics in mouse models of disease contributes to the quantification of both the normal physiology and that of disease progression. Micro-ultrasound provides such utility, allowing for the mapping and visualization of tumour vasculature using power Doppler which can detect blood flow ranging from $2\,\mathrm{mm\,s^{-1}}$ up to $4\,\mathrm{m\,s^{-1}}$ in tumours at multiple time points [87–89]. Power Doppler can be used to detect subtle changes in tumour perfusion and blood vessel architecture in a

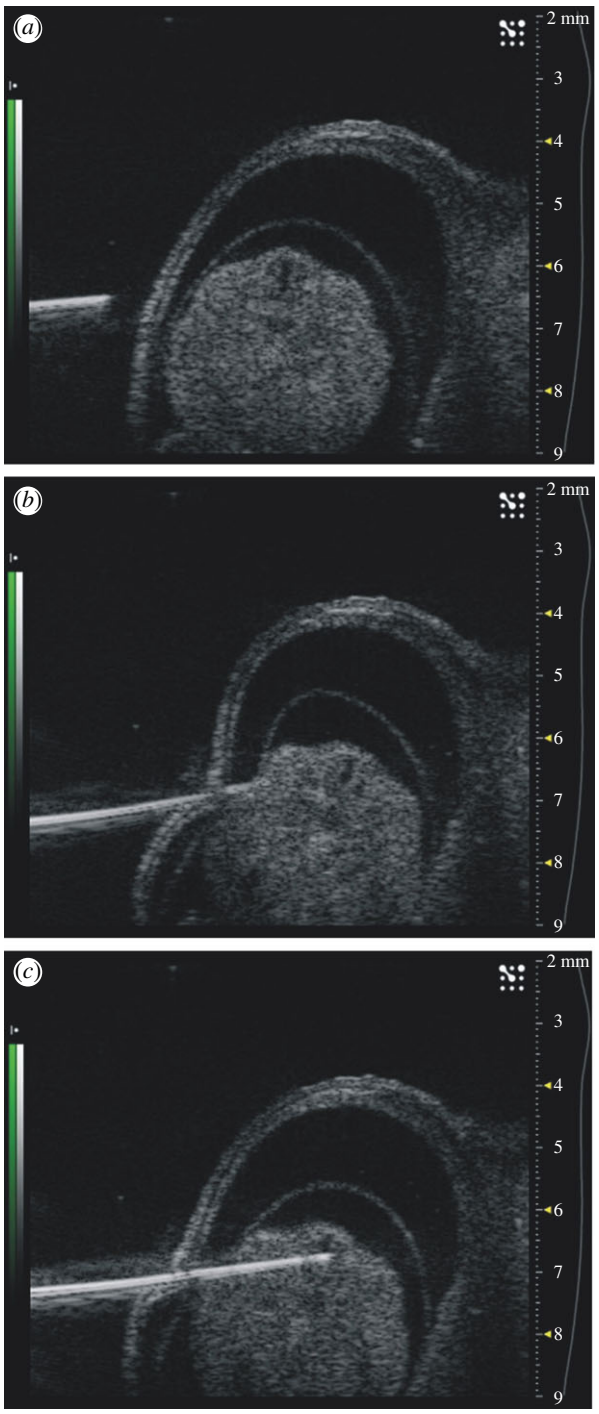

Figure 10. Ultrasound guided microinjection into the spinal canal of a mouse embryo. Progressive penetration to the target tissue is shown (a–c). The elastic nature of most tissues makes guidance challenging as shown in (b) where deformation significantly modifies the projected trajectory.

non-invasive longitudinal manner. Xuan *et al.* [89] reported the application of high-frequency three-dimensional power Doppler micro-ultrasound imaging in a genetically engineered mouse prostate cancer model. They showed that three-dimensional power Doppler could reproducibly depict functional neoangiogenic blood flow in prostate tumours when compared with normal prostate tissue which had less flow. These observations were confirmed using micro-computed tomography and by correlation with microvessel distributions measured by immunohistochemistry and enhanced vascularity visualized by confocal microscopy. Further evidence of the concordance of non-invasive micro-ultrasound measurements with CD31 and other immunohistochemical stains is given by Franco *et al.* [90], Shaked *et al.* [28] and Cheung *et al.* [24].

4.3. Micro-ultrasound in studies of therapeutic interventions

The systematic investigation of new therapies and combinations of therapies can be conducted to inform the development of strategies suitable for clinical investigation. From the clinical point of view, imaging tools for the microcirculation offer the potential to characterize disease progression and determine response to therapy enabling timely modifications to the therapeutic strategy. Imaging findings may also carry prognostic information that is important for patient management. A key component of studying cancer in animal models is understanding how specific drugs affect angiogenesis. Studies by Goertz *et al.* [87] reported the first use of high-frequency micro-ultrasound two-dimensional power Doppler in studying the effects of an antivascular drug on blood flow. The authors reported a significant reduction in blood flow in superficial human melanoma MeWo tumours 4 h after injection of the tumour vascular targeting agent ZD6126 followed by a recovery of flow by 24 h after injection. A study from Jugold *et al.* [88] investigated the effects of blocking VEGF mediated pathways using a VEGFR-2 blocking antibody treatment. Using power Doppler imaging, this study showed that after 6 days of treatment in subcutaneous tumours (spontaneously immortalized human skin keratinocytes) in nude mice, tumour vascularity significantly decreased. The consequences of anti-VEGFR-2 treatment in MDA-MB-231 breast cancer tumours by Franco *et al.* [90] concluded that sustained hypoxia and impaired vascular function were consistent findings in this model. The administration of antiangiogenic agents or signal blocking molecules does not always result in decreases of flow. Qayum *et al.* [91] showed this in a fibrosarcoma model following treatments that blocked oncogenic signalling molecules such as EGFR, PI3K, RAS and AKT. Their work showed prolonged, durable enhancement of tumour vascular flow. This is relevant for treatment in that it may be desirable to increase flow to facilitate chemotherapeutic therapy. Olive *et al.* [27] examined this hypothesis in a study in which gemcitabine was co-administered with a hedgehog signalling inhibitor (IPI-926) in a mouse model of pancreatic cancer. Micro-ultrasound validated increases in perfusion and disease stabilization using this approach. Shaked *et al.* [28] used micro-ultrasound to examine a therapy consisting of sequential use of a vascular targeting agent (Oxy-4503, Oxygene Inc.) and anti-VEGFR-2 therapy (DC101, Imclone Inc). Their results showed that the use of the antiangiogenic agent post-antivascular treatment significantly impaired recruitment of circulating endothelial cells and subsequent revascularization of the tumour periphery. Micro-ultrasound is playing an increasing role in these evaluations of combination therapies.

4.4. Contrast imaging

The numerous approaches developed at clinical frequencies (§2.2) for MB contrast imaging can effectively be applied to cancer models in the mouse at higher frequencies. This allows the non-invasive assessment of relative perfusion and blood volume without the need for tissue extraction, immunohistochemical staining and vessel counting. Examples of B-mode images of MB contrast following the injection of 80 µl of MicroMarker (VisualSonics, Toronto) contrast into the tail vein of a mouse bearing a Lewis lung carcinoma are given in figure 11. Imaging is performed with a Vevo 2100 scanner using nonlinear contrast mode at 20 MHz. At time $t = 0$ (figure 11*a*) only the outline of the tumour is visible with the tumour signals suppressed by the nonlinear processing. At 1 s, the larger arterioles are visible as a branching pattern of vasculature beginning to fill the tumour (figure 11*b*). By 5 s, the tumour has filled with contrast but the filling rate and distribution are not completely homogeneous (figure 11*c*). This inherent tumour heterogeneity can be analysed by selecting regions of interest (ROIs) in the B-scan as indicated in figure 12*a* and plotting the contrast power as a function of time as in figure 12*c*. The maximum slope of the wash-in phase is considered to be proportional to perfusion whereas the peak or plateau value is proportional to blood volume. In this case, the analysis indicates that one region (red outline) has less perfusion and vascular volume than the region outlined in green. Fits to the wash-in kinetics are also given in figure 12*c*. These fits are based on lognormal distributions and include secondary effects such as 'second pass' circulation of the MBs. The fits, in this case, can be observed to deviate from these distributions indicating a need for improved models such as those developed by Hudson *et al.* [92]. Pixel by pixel analysis of wash-in fits can be transformed into parametric maps reporting haemodynamic information such as blood volume (figure 12*b*).

The value of being able to report relative changes in perfusion and blood volume lies in the interpretation of biological responses to new therapies designed to manipulate the angiogenic microcirculations of growing tumours. Sunitinib, for example, is a receptor tyrosine kinase inhibitor with broad specificity for signalling in the angiogenic cascade. One of the clinical observations has been that patients' tumours 'rebound' in the two week off cycle following four weeks on the drug. Figure 13 shows an attempt to demonstrate this in a mouse model of MDA-MD-231 breast cancer. Groups of 5–8 mice with implanted tumours were studied with MB techniques as described above. Mice were treated with 80 mg kg^{-1} sunitinib by gavage daily for one week and were imaged with contrast at the onset of treatment, at the completion of treatment, and one and two weeks following cessation of treatment. The results are shown in figure 13. Ultrasound measured growth rates show that the tumours of treated mice grew less rapidly than control. Analysis of tumour blood volume showed significant suppression after one week but a significant rebound effect (figure 13, arrows) one week after therapy terminates. Note also, paradoxically, that while the treatment is considered antiangiogenic and does suppress flow over the treatment period, blood flow is ultimately higher in treated animals than controls and tumour control is better. This leads to important questions regarding the use of contrast ultrasound as an early predictor of response. Both preclinical and clinical studies are ongoing in this area.

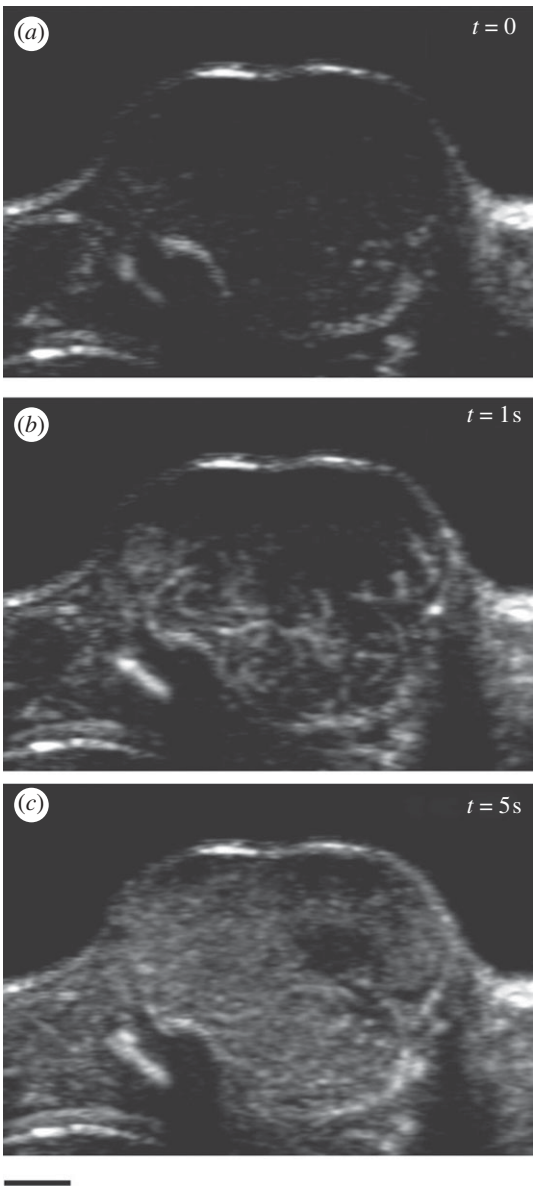

Figure 11. Wash-in of MB contrast at $t = 0$ s (*a*), 1 s (*b*), and 5 s (*c*) following a tail vein injection of 80 µl MicroMarker contrast. Lewis lung carcinoma Swiss nude mouse. Probe: MS250. Scale bar, 2 mm.

4.5. Molecular imaging of angiogenesis

MB contrast agents are confined to the blood pool. This makes them ideal agents for the assessment and evaluation of molecular markers associated with angiogenesis. The techniques to create targeted MBs have been developed over the past decade. Following the pioneering work of Lanza [93,94], Unger, Lindner, and

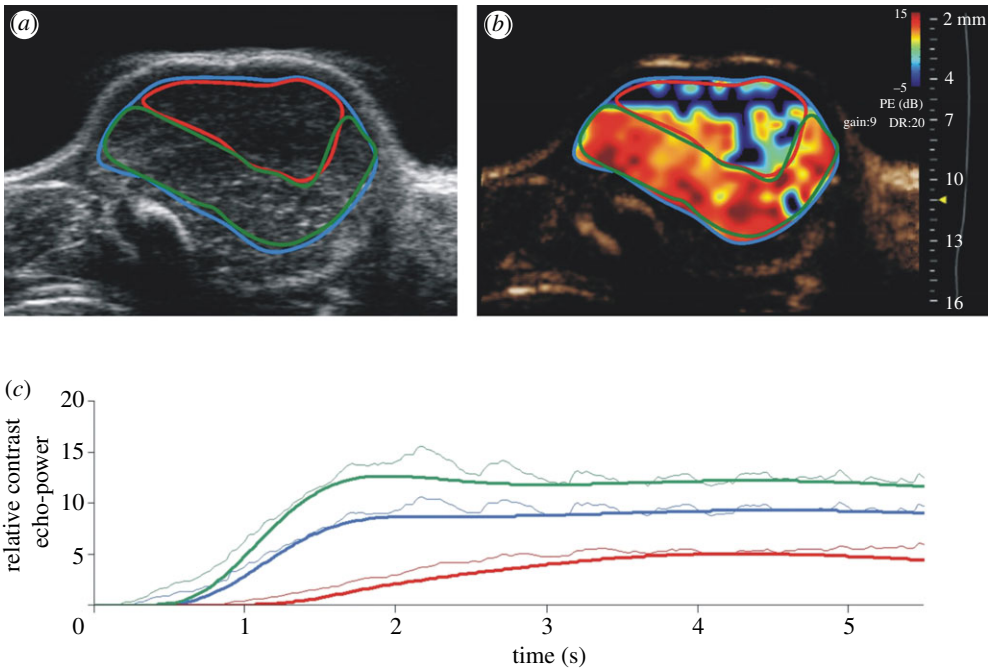

Figure 12. (*a*) Identification of ROIs in the Lewis lung carcinoma of figure 11. (*b*) Parametric map of relative blood volume (based on the peak of the wash-in curve) overlaid on the contrast image. (*c*) Wash-in kinetics of the three ROIs in (*a*).

Klibanov [95–97], commercial formulations of MBs were developed in which ligands for endothelial cell surface markers were attached to the shell. Specific ligands for markers of angiogenesis, inflammation and thrombin enable the MBs to attach as a consequence of random encounters with endothelial cell surface targets. The availability of molecular contrast kits (VisualSonics Inc., TargetReady MicroMarker; Targeson Inc., Targestar) has facilitated the investigation of a wide range of molecular targets including VEGFR-2, VCAM, MadCAM, endoglin and glycoprotein IIb/IIIa. Once MBs are attached to their targets they are more stable than circulating MBs and can be imaged using micro-ultrasound resulting in a molecular map proportional to endothelial cell or thrombin receptor density. The time sequence for molecular imaging of mice is illustrated schematically in figure 14*a*. MBs bearing the appropriate ligand for the chosen target such as an anti-VEGFR-2 antibody or an isotype control antibody are administered via a tail vein or jugular cannula. MBs are usually administered as a bolus of 5×10^7 particles in approximately 50 µl followed by a 20 µl saline flush. MB wash-in within the tumour is measured by imaging at low power (10%) immediately following administration and results in a contrast wash-in curve. Targeted MBs are allowed to accumulate for approximately 4 min as indicated in figure 14*a*. At this time several seconds of image data are recorded at low power to avoid MB disruption, and a high-power disruptive pulse sequence is applied. The disruptive sequence serves to eliminate MBs within the beam elevation. Immediately after the disruption sequence, imaging is re-commenced at low power, and residual circulating MBs are observed to replenish the beam. The molecular signal is defined as the difference between pre- and post-disruption signals. An example of the molecular signal for a region of a breast cancer orthograft is given in figure 14*b*. Subtraction of the post-disruption image from the pre-disruption image therefore results in a molecular image. This image data may be superimposed as on

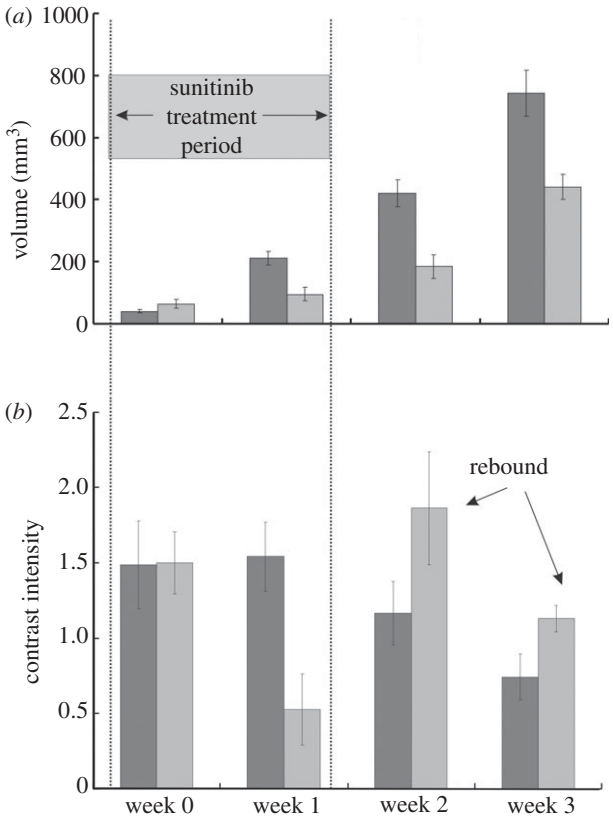

Figure 13. Orthotopic breast tumour growth and relative blood volume measured using MB contrast infusions following a one week treatment regimen with Sutent (sunitinib) at 80 mg kg^{-1} d^{-1}. (*a*) Tumour growth, (*b*) blood volume. Black bar, control; grey bar, treated.

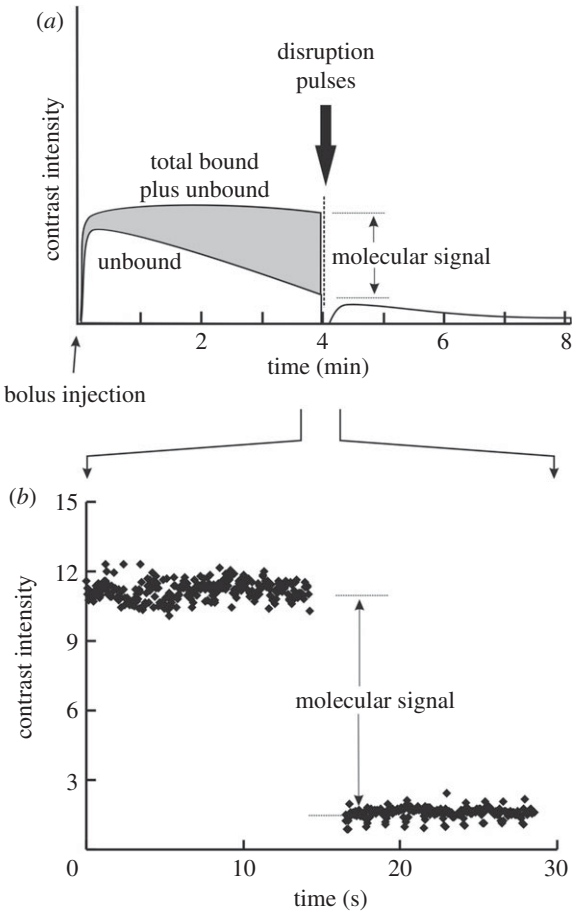

Figure 14. (*a*) Schematic of a molecular imaging experiment. At time $t = 0$ a bolus of contrast is injected in the tail vein of the mouse. As the signal due to bound contrast increases the unbound agent is cleared by the lungs, liver and spleen. At 4 min a disruption pulse eliminates the contrast in the imaging plane after which only circulating MBs are detected. The difference between pre- and post-disruption is a representation of the 'molecular signal'. (*b*) Actual signal for a breast cancer orthograft (MDA-MB-231) following a 50 μl injection of VEGFR-2 targeted MBs (1.02×10^9 MB ml^{-1}).

the greyscale image to provide a graphic indication of molecular binding. High frequency 'molecular' images of VEGFR-2 in melanoma xenografts are shown for four different tumours implanted in mice in figure 15. Note that in contrast to lower frequency molecular imaging, the molecular labelling appears to be confined to discrete vascular channels that are readily visible in shades of green. The high resolution of micro-ultrasound molecular imaging is unique among the molecular imaging techniques in that the technique allows simultaneous high morphologic tissue and molecular resolution. Quantification of molecular targets (VEGFR-2) with micro-ultrasound was first demonstrated by Rychak *et al.* [98] in melanoma models. Lyshchik *et al.* investigated the use of a new targeted MB in which streptavidin was directly linked to the MB. This agent (MicroMarker, VisualSonics Inc., Canada) was used to successfully image VEGFR-2 expression in mouse models of breast cancer [84]. In particular, they showed differences in VEGFR-2 expression patterns between highly invasive metastatic (4T1) and non-metatstatic (67NR) breast cancer tumours. Willmann *et al.* recently provided additional validating evidence for targeted imaging of VEGFR-2. Beginning in 2008 studies of MB binding and expression in cell culture and in mouse angiosarcoma and rat malignant glioma studies confirmed the specificity of targeting VEGFR-2 using the MicroMarker agent [99]. They investigated the whole-body distribution of targeted MBs using radiolabelled antibodies and found, in addition to strong uptake in mouse angiosarcomas, rapid uptake in the liver and spleen [100]. Blood clearance occurred after 3.5 min further validating the 4 min wait for molecular imaging indicated in figure 14*a*. Willmann's group also investigated the potential of dual targeted agents for $\alpha V\beta 3$ and VEGFR-2 showing improved *in vivo* visualization of tumour angiogenesis in a mouse model of ovarian cancer [101]. Recently, they have further demonstrated the potential of high-frequency molecular imaging using a clinically translatable MB (BR-55, Bracco Inc.) that replaces the strepavadin–biotin linker with a small heterodimeric peptide that targets VEGFR-2 [102]. Results in cell culture and mouse tumours bode well that this may be the first targeted ultrasound contrast agent for the clinic [102].

5. APPLICATIONS: CARDIOVASCULAR IMAGING

Ischaemic heart disease is the subject of extensive worldwide research in hundreds of cardiovascular laboratories. Basic cardiovascular research relies heavily on the mouse species for providing a highly characterized and widely accepted model for human cardiovascular disease. The use of transgenic and knockout mice has provided new understanding of the genetic, molecular and cellular mechanisms underlying every major cardiovascular disease including: atherosclerosis, hypertension and diabetes—resulting in significant drug discovery in these areas [103]. There are significant surgical challenges involved with the induction of a realistic myocardial infarction (MI) in mice and it is only in relatively recent years that reliable approaches have been developed [104–107]. Early research frequently relied heavily on immunostaining tissue samples, and, for assessing heart function, performing tedious invasive catheter-based measurements of left ventricular (LV) pressure. Significant limitations of these non-imaging methods include the inability to non-invasively quantify (i) LV dimensions, (ii) global/regional function, and (iii) infarct size at the beginning of an LV remodelling study.

Since the wall thickness of the mouse myocardium is approximately 1 mm, this suggests that a spatial resolution in the range 50–100 μm is preferable. (Wall thickness in a post-MI 'remodelled' mouse heart LV may be considerably less than 1 mm lending further emphasis to the need for a less than 100 μm resolution.) The heart rate is approximately 650 beats per minute (b.p.m.) in an awake mouse whereas different classes of anaesthesia reduce the heart rate to 300–400 b.p.m. [108]. This suggests the use of an acquisition imaging frame rate in the range 120–150 Hz [109]. It is also observed that whereas most mouse cardiac studies will

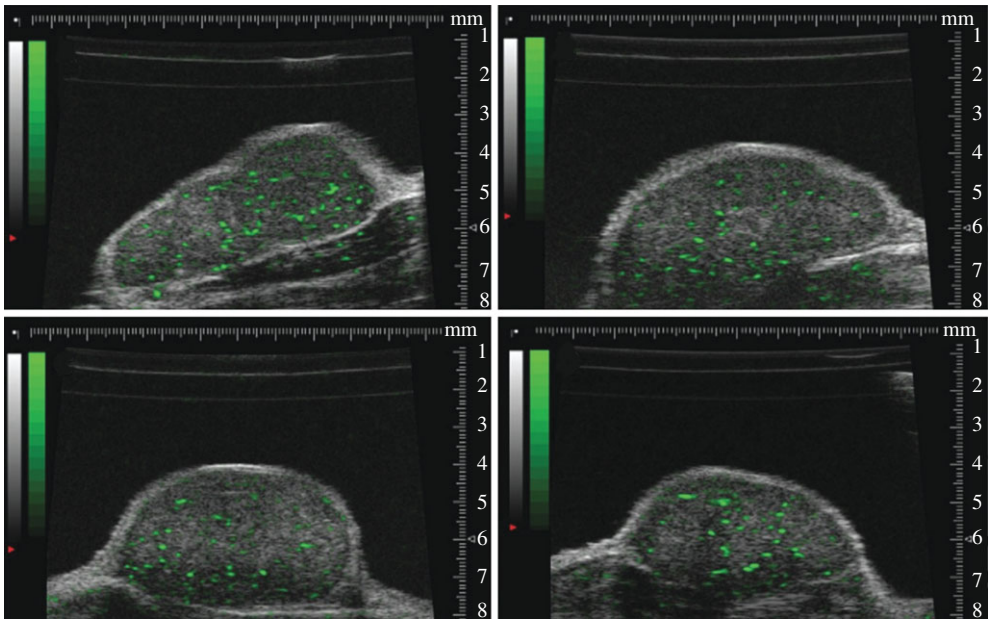

Figure 15. Molecular imaging of four different mice bearing melanoma (MeWo) xenografts. Bound MBs targeted to VEGFR-2 are displayed on a green colour scale and overlaid on B-mode images.

involve an anaesthetized mouse, there are compelling reasons to have the capability to perform a study in awake mice. Yang *et al.* [108] have demonstrated that imaging of awake mice can be achieved after gaining the necessary operator experience and training the mouse to tolerate awake scanning. In addition to the impact of anaesthesia on haemodynamic status and function of the heart, a very sick mouse may not survive anaesthesia. Having outlined the primary desired specifications of an imaging system, it is evident that dedicated high-frequency ultrasound imaging is practically essential for reliable, accurate, non-invasive assessment of murine cardiac function [109]. Although there have been many notable contributions to the field of murine echocardiography using clinical scanners operating at their highest operating frequency (generally in the vicinity of 14 MHz), the scope of these contributions is frequently limited, to varying degrees, by raw imaging resolution (typically approx. 100 μm axial and approx. 200 μm lateral resolution). It would appear that many findings previously made using approximately 14 MHz may be usefully improved upon by repeating them at 30 MHz. It is also worth observing that it is unlikely that frequencies significantly higher than 30 MHz will be used in the near future for adult murine cardiac imaging. Higher frequency transducers are available but do not outperform 30 MHz in adult murine echocardiography due to a combination of reduced imaging penetration and a greater susceptibility to image defects arising from imaging through the chest wall (i.e. ribs, sternum, etc.). In the longer term, it is feasible that advanced signal processing techniques, such as those using coded waveforms, may extend imaging penetration at higher frequencies. However, there appears to remain, for the time being, a role for lower frequency imaging at least in the context of MB imaging where higher MB signal sensitivity and specificity may be traded for inferior spatial resolution.

Zhou *et al.* [22], using VisualSonics Vevo 770 instrumentation, have described useful, practical, scanning techniques and acoustical 'windows' that are optimal in mouse cardiac imaging. Zhou *et al.* also demonstrated the use of high-resolution ultrasound to measure the dimensions of the LV and ascending aorta and obtained Doppler flow at six representative intracardiac locations (right superior vena cava, tricuspid orifice, main pulmonary artery, pulmonary vein, mitral orifice, and ascending aorta). Remarkably, it was demonstrated that the approach could resolve anatomy and haemodynamics in the heart right down to the coronary arteries. Figure 16 taken from that work shows imaging and Doppler of the right (figure 16*a,b*) and left inflow channels (figure 16*d,e*) with magnetic resonance images as correlates (figure 16*c,f*).

It is worthwhile briefly considering the potential of magnetic resonance imaging (MRI) as an alternative to high-resolution ultrasound in the context of cardiac imaging. Assessment of cardiac function using small-animal MRI has been performed for many years now [22] but the cost of MRI (capital cost and cost per scan) places it beyond the reach of all but a few cardiovascular research laboratories. Additionally, the long duration (approx. 1 h) of typical cardiac MRI scans necessitates extended anaesthesia that can put an unwelcome stress on a sick mouse. Long scan times also severely limit scanning 'throughput' in shared equipment settings involving multiple parallel studies. However, MRI is generally considered to be less susceptible to serious image artefacts that may result in a 'technical failure' in an imaging procedure. Reduction of the incidence of artefact in cardiac ultrasound, such as static reverberation artefact overlying moving tissue, is a fruitful area of on-going research [110,111]. Reductions in the incidence of imaging artefacts are particularly relevant to the conduct of serial studies since each imaging failure can result in the elimination of a particular individual, and all its previously acquired

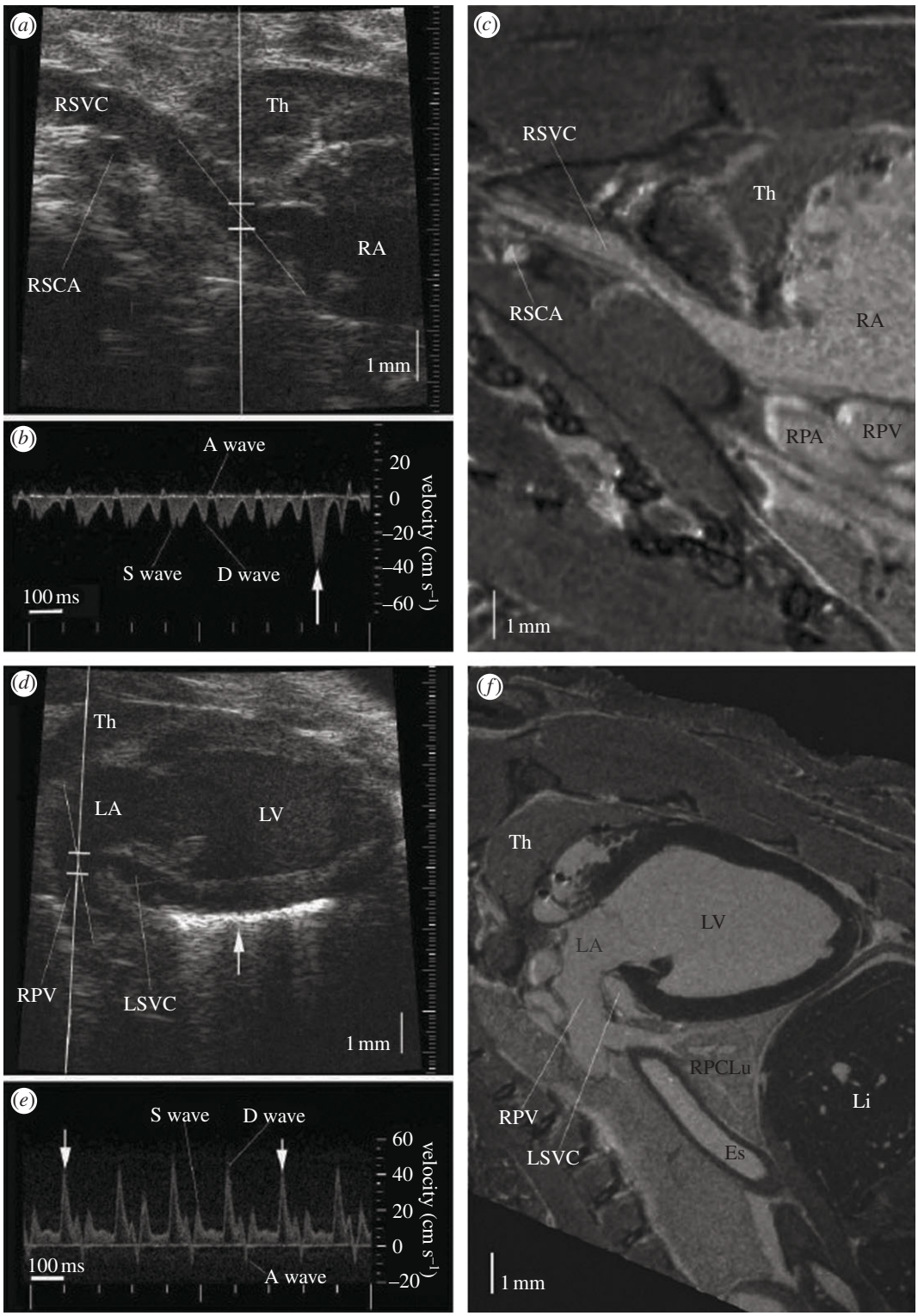

Figure 16. Micro-ultrasound imaging of the right and left atrial inflow channels, with anatomical confirmation by magnetic resonance (MR) imaging. (*a*) Image of a right parasternal longitudinal section. (*b*) The Doppler flow spectrum of right superior vena cava (RSVC), showing a small retrograde wave caused by atrial contraction. (*c*) MR image of a similar section to the micro-ultrasound image in (*a*), showing the vascular continuity from RSVC to the right atrium (RA), and the surrounding organs such as thymus (TH), right subclavian artery (RSCA), right pulmonary artery (RPA) and right pulmonary vein (RPV). (*d*) The micro-ultrasound image of a left parasternal longitudinal section showing the RPV, LA and LV, with the Doppler sample volume in the entrance of the RPV. (*e*) The Doppler flow spectrum from PV. The arrows indicate heart beats at the end of inspiration. (*f*) The MR image of a similar section to the micro-ultrasound image in (*d*). Adapted from [22].

data, from subsequent statistical analysis. A consequence of this problem is that it necessitates the use of a poorly predicted larger initial sample count that might not be feasible at all in the case of unique genotypes.

5.1. Quantification left ventricular function

Since the primary function of the LV is to pump volumes of freshly oxygenated blood according to

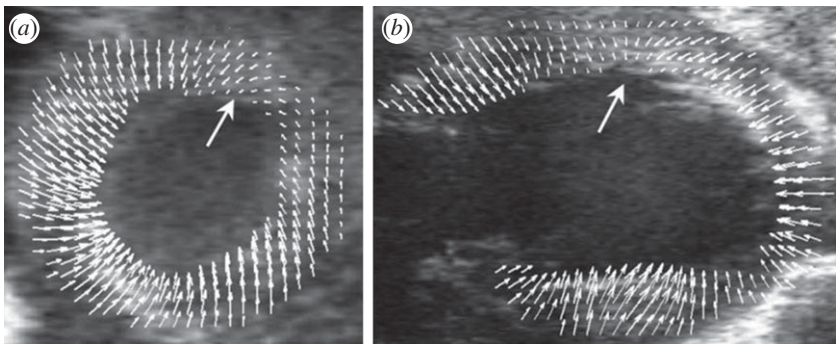

Figure 17. Displacement maps for a day 1 post-MI mouse heart superimposed onto the original ultrasound images to provide a visual representation of the relationship between anatomy and function. (*a*) Mid-ventricular, short-axis view. (*b*) Long-axis view of a second day 1 post-MI mouse heart. Wall motion defects, involving reduced regional displacement, are indicated with large arrows. Adapted from [112].

physiological demand, a variety of metrics can be developed to assess the functional performance of the LV. These metrics broadly correspond to those widely used in clinical echocardiography. The advantages and disadvantages of various metrics, and the degree of complexity associated with their acquisition, also correlate with clinical experience. For example, estimates of chamber volume employing a single one dimension versus time measurement (e.g. M-mode) are, in both small-animal imaging and clinical practice, the quickest and easiest to acquire but also the least accurate and repeatable. The review paper associated with Scherrer-Crosbie's Feigenbaum Lecture [109] contains a comparison of M-mode images acquired at 7, 13 and 30 MHz, demonstrating the finer resolution at higher frequencies, and also draws attention to an example in which post MI remodelling was detectable in B-mode but not in M-mode. This is explained by the fact that LV remodelling usually results in a highly heterogeneous LV that is susceptible to error when attempting to estimate a ventricular metric (e.g. LV chamber volume) using a single linear measurement as is the case in M-mode. Since serial study is a common element in cardiovascular research, most researchers find that more sophisticated measures of volume, relying on two- or three-dimensional measurements, are necessary to reduce measurement noise and improve statistical quality.

Current mouse ultrasound instrumentation is based upon two-dimensional B-mode scans and therefore the extension to three dimensions usually involves making a systematic sequence of scans through the heart volume by scanning precisely in elevational increments. Usually, this involves a 'breadslice' sequence of short axis (SA) views from LV base to apex with a step size typically in the range 0.5–1.0 mm. It is conceivable that, following the practice in current clinical echocardiography, a two-dimensional high-frequency array acquiring three-dimensional data directly will be developed in the future. However, for practical and economic reasons, it is anticipated that a real-time three-dimensional imaging capability for mouse imaging is several years away.

In the past 10 years, various forms of tissue tracking, or 'speckle tracking' have been applied in clinical echocardiography to assess LV function. Conceptually, these methods derive from feature matching a matrix of small image regions through the cardiac cycle. Typically, in mouse cardiac imaging, pixel blocks encompassing a few speckles (e.g. 0.2 mm^2) are defined and tracked using cross correlation, minimum sum of absolute differences, or similar matching algorithms [112]. When only the LV chamber volume is being measured, it is only necessary to track the endocardial border. Since the endocardial border is a blood–tissue interface, it appears as an enhanced brightness feature that is readily amenable to tracking and is generally a more reliable image feature than intra-myocardium tissue that is more susceptible to image dropout.

From a research viewpoint, tracking only the endocardial border is ignoring a rich set of data that may be derived from tracking tissue motion within the myocardium itself. By defining a matrix of image regions across the myocardium, a finely spaced matrix of tissue displacements may be derived [112,113] as illustrated in figure 17. Once the displacements are obtained in rectangular (Cartesian) coordinate space, LV myocardial displacements may be decomposed into radial and circumferential components [112]. Thereafter, the gradient of the displacements is employed to obtain local myocardial strain [112,113]. Quantitative calculation of local tissue elasticity requires knowledge of pressure information in the LV and the added complexity is not well justified since a mapping of strain is sufficient to highlight most forms of regional dysfunction. Tissue tracking using ultrasound has been successfully validated against matched MRI DENSE tracking data [112] as shown in figure 18. Several researchers have examined approaches for optimizing tissue tracking in the mouse LV. Luo *et al.* [114] describe manual initialization of the myocardium (i.e. the region to be tracked). Thereafter, the tracked ROI is automatically updated based on the tissue tracking itself. An important application of tissue tracking and quantification of LV contraction is for detecting and characterization of the extent of MI [114]. Tissue tracking frequently involves the use of scan converted, processed, video output data. However, the use of radio frequency ('raw') data has also been examined [115]. Radio frequency data enable finer resolution tissue tracking, especially when tracking parallel to the ultrasound beam axis.

One approach to obtaining a finely sampled comprehensive three-dimensional dataset involves acquiring

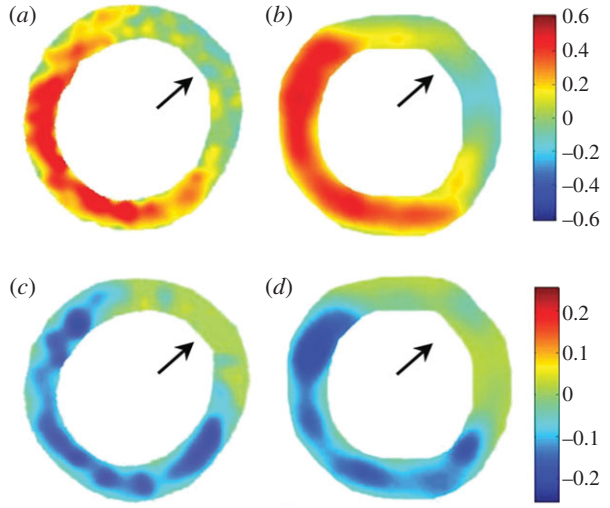

Figure 18. End diastole (ED) to end systole (ES) E_{rr} (radial) strain maps from a day 1 post-MI mouse heart using MRI (*a*) and ultrasound (*b*). ED-to-ES E_{cc} (circumferential) strain maps from the same mouse heart using MRI (*c*) and ultrasound (*d*). In both the E_{rr} and E_{cc}, maps, defects in contraction are observed in the anterolateral LV (as indicated by arrows). Adapted from [112].

sets of orthogonal planes [116]. A sequence of SA slices and sequence of long axis slices are acquired. Along the lines of intersection of these planes, one can obtain all three displacement components (with redundancy in the axial direction). Within each acquired plane one can obtain a fine sampling of two-dimensional displacement components or use estimates out of plane motion based on rate of signal decorrelation [116]. Using interpolation, it is then feasible, in principle, to achieve a longstanding goal of obtaining a comprehensive, finely sampled, set of three-dimensional displacements through the entire LV.

An interesting derivative of strain imaging involves examining the evolution of the contraction of the myocardium [117,118]. Contraction is induced by a fast propagating electrical wave that results in a propagating mechanical wave that is measurable using ultrasound by analysing the relative delay of contraction among adjacent tissue regions. Examples of such images are given in figure 19. The mechanical wave velocity was found to be approximately 0.87 $\mathrm{m\,s^{-1}}$ in the posterior LV wall of a control mouse but the velocity of this wave reduced to 0.66 $\mathrm{m\,s^{-1}}$ in the case of an induced ischaemic region [117]. Broadly similar analyses have also been used to measure the pulse wave velocity in the carotid arteries of mice [119]. Vessel wall pulse wave velocity is a function of wall stiffness and density and therefore an indirect measure of arterial stiffness is obtained from detectable wave velocity. Vessel wall stiffness is related to overall vessel health and haemodynamic resistance. Using similar approaches, Fujikura *et al.* [120] have reported successful assessment of regional mouse aortic wall stiffness using the natural mechanical, pulsating motion of the mouse aorta using high-resolution ultrasound imaging.

Systolic dyssynchrony describes a lack of coherence in the systolic phase among various LV wall segments resulting in loss of pump efficiency. In the past, M-mode echocardiography has been frequently used to examine the time delay between peak inward septal and posterior wall movement [121]. Clearly, M-mode imaging is limited by virtue of the fact that it only analyses a single beamwidth that intersects with proximal and distal wall segments and does not encompass the entire LV wall. Following the precedent in clinical echocardiography, several groups have examined automated two-dimensional myocardial tracking as a method for deriving quantitative metrics for LV function using speckle tracking across a sequence of images through the cardiac cycle. The degree of regional synchrony, or dyssynchrony, may be assessed by comparing the time course of tracked motion for a set of regions around the circumference of the SA view. Reflecting the importance of understanding the evolution of dyssynchrony following MI as precursor to longer term LV wall remodelling, Li *et al.* [122] have examined the pattern of dyssynchrony in mice.

5.2. Microbubble contrast perfusion imaging

Early use of MB-based ultrasound contrast agents primarily focused on their use as a tracer for blood flow and therefore as a means to assess tissue perfusion. In cardiac applications, the method is frequently referred to as myocardial contrast echocardiography (MCE). In many respects, the use of ultrasound contrast agent as a means of perfusion assessment in cardiac imaging is similar to its use in assessing cancer perfusion. Scherer-Crosbie *et al.* [123] describe a typical example of the use of MB methods to assess perfusion in a post-MI LV for the purpose of developing a non-invasive real-time estimate of area at risk (AAR). A reasonably good correlation between AAR derived using contrast and a histological reference using fluorescent microspheres was obtained (contrast derived AAR = 0.75 microspheres derived AAR, $r^2 = 0.78$; $p < 0.0001$). It is possible to repeat the process on a stack of adjacent SA slices to estimate a three-dimensional perfusion map of the entire LV. This has been performed using both fluorescent microspheres [123] and conventional histological staining using phthalo blue dye to identify perfused regions [124]. Perfusion imaging may use a bolus injection (producing a short lived, but intense echo signal) or use a continuous slower perfusion that is periodically interrupted by high intensity ultrasound that clears practically all MBs in the field of view. Using the initial slope of contrast refill, versus time, estimates of blood perfusion may be made [125]. One interesting variant of conventional contrast agent (typically approximately 1–3 μm in diameter) involves the use of large diameter 'depot' agent (more than 5 μm in diameter) that lodges in the capillaries [126]. Infarct size determined by imaging of lodged 'depot' agent correlated well with histological analysis of previously infused fluorescent nanospheres ($r = 0.94$, $p < 0.001$).

5.3. Cardiac molecular imaging using targeted microbubbles

Although the basis of molecular imaging using ultrasound contrast agents is well known and described

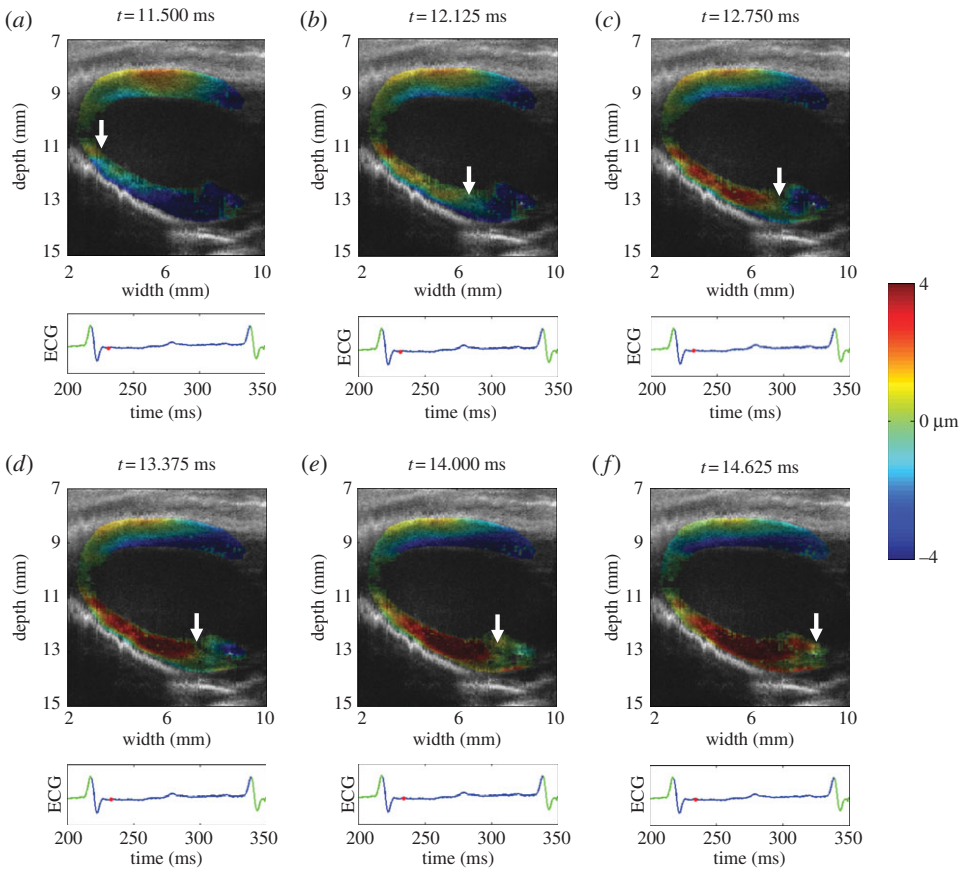

Figure 19. Sequence of electromechanical displacement images every 0.625 ms in a normal mouse left ventricle during sinus rhythm. The displacements are colour-coded and overlaid onto the B-mode images. Positive displacements (in red) represent upward motion, which negative displacements (in blue) represent downward motion. The arrows indicate the propagation of the electromechanical activation from the apex to the base along the posteriolateral wall.

previously in §§2.2, 4.4 and 4.5, it is only relatively recently that this approach became feasible practically *in vivo* in small-animal cardiovascular research [127]. Ultrasound molecular imaging uses contrast agents with specific ligands coupled to the bubble surface that recognize selected surface receptors present on the endothelium. Contrast agents, administered intravenously to the subject, selectively attach to the receptors of interest and accumulate in the regions of disease. MB detection sensitivity with currently approved clinical imaging equipment is excellent, and single contrast particles (i.e. picogram mass) are detectable [128]. However, as noted earlier in this article, achieving optimal sensitivity and specificity at the frequencies desired for small imaging remains a challenge and a very worthwhile area for further innovation and development.

Convenient and efficient methods for the attachment of targeting ligands (usually antibodies) to these particles have been developed [129]. These ligand-coated MBs bind to receptor-coated surfaces, such as P-selectin-coated plastic [130] or activated endothelium that displays ICAM-1 molecules on its luminal surface [131]. Kaufmann *et al.* [132] examined the potential to image vascular inflammatory responses using VCAM-1 targeting and concluded that the approach was capable of detecting and quantifying vascular inflammatory changes that occur in early stages of atherosclerosis [133]. The technology of ligand attachment and overall strategy for achieving successful and robust molecular ligand–receptor binding in the presence of the high flow rates encountered in larger vessels is an area of active research [134]. Klibanov [135] has written an article describing the underlying principles of MB design including details of molecular targeting strategies. It is also worth noting that a search on the use of molecular targeted contrast will produce many more articles than one focusing on non-targeted MBs for assessing perfusion. In this respect, the field has progressed very rapidly in the past 5 years. Additionally, a new extension of MBs for molecular imaging involves exploiting them in a dual role for both imaging and localized drug delivery [136]. Clearly, small-animal models will play an important role when examining the potential for new methods for focal drug delivery. It is also worth noting that although the frequencies of high-resolution ultrasound systems are poorly matched to the natural resonance frequencies of commonly encountered MBs, existing instruments (including even intravascular ultrasound catheters) have the capacity to break MBs and affect drug/gene delivery [137].

5.4. Measurement of flow using Doppler techniques

Similar to other examples in mouse echocardiography, early Doppler flow work simply relied upon high-frequency clinical scanners operating the highest available Doppler frequency for both colour Doppler

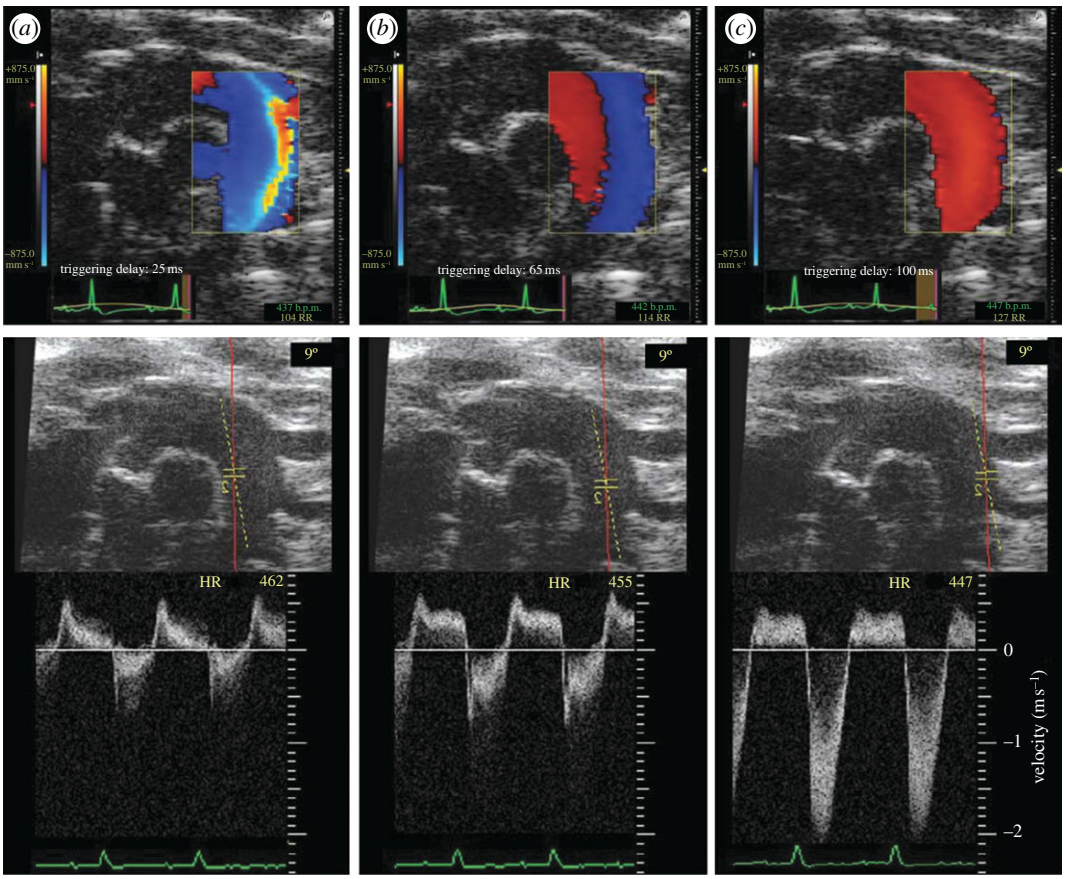

Figure 20. Flow distribution in the aortic arch in a $ldlr^{-/-}$ mouse with surgically induced aortic regurgitation. (*a*) The Doppler colour flow frame at the peak systole showing the antegrade flow in blue with the higher velocity along the greater curvature and the lower velocity along the lesser curvature. (*b*) The frame at the early diastole showing the retrograde flow (red) along the lesser curvature, when the flow along the greater curvature is still moving forward (blue). (*c*) The frame at the middle diastole showing the retrograde flow (red) in the whole aortic arch. The Doppler flow spectra recorded along the lesser curvature, at the middle lumen and along the greater curvature in the aortic arch show the altered haemodynamics associated with the regurgitation. Adapted from [141].

and pulsed wave Doppler [138,139]. However, Hartley *et al.* [140] developed special purpose non-invasive 20 MHz probes for accurately assessing blood flow velocities in the mouse aorta and for measuring the pulse wave velocity of the aorta. More recently, the advent of micro-ultrasound instruments has greatly facilitated fine resolution Doppler measurements that include power Doppler, colour Doppler and B-mode duplex imaging. These instruments have made significant contributions to the study of haemodynamics and its effect on plaque distribution in models of atherosclerosis. Figure 20 beautifully shows colour flow, B-mode and pulsed Doppler waveforms for the aortic arch of a low-density lipoprotein knockout mouse with surgically induced aortic regurgitation [141]. A flow separation is clearly evident in the colour flow and Doppler data of figure 20*b*. Significant regurgitant flow is seen in figure 20*c* during the diastolic phase of the heart cycle.

5.5. *Assessing impact of disease, contaminants and genetics on the mouse heart*

Once the instrumentation and experimental techniques for conducting high-resolution imaging of the mouse heart are developed and available, it becomes readily feasible to examine the impact of various drugs, contaminants or disease states. In many cases, it becomes of interest to examine various permutations of drug dosing and response at a selected set of time points. As noted above, the ability to track evolution of response within a single animal is very important from a cost and accuracy viewpoint. Only a very sparse sample of studies are briefly reviewed here. Kanashiro-Takeuchi *et al.* [142] examined the impact of trichloroethylene (TCE), an organic groundwater contaminant, on *in ovo* chick embryos. At ED5.5, it was observed that TCE-exposed hearts possessed functional and morphological heterogeneity that impacted heart rate, LV mass and wall thickness. Shamart *et al.* [143] examined whether diabetes alters cardiac fibroblast activity in the myocardium in a six-week streptozotocin-induced type 1 diabetic mouse model. High-frequency ultrasound of the heart revealed significant dilation of the LV in the diabetic animals.

One of the most important unique features of a mouse model for human disease is that it is amenable to genetic modification and consequently it is possible to examine the role of specific genes in various aspects of cardiac disease. Since some new genotypes are not even viable to birth, or have a high rate of mortality in infancy, it is readily evident that there is a high value attached to the ability to non-invasively assess morphology and function accurately and reliably at the very earliest opportunity *in utero* and through

development as described in §3.4. There is a rapidly growing literature involving the use of high-resolution ultrasound to assess the relationship of genetics to cardiovascular morphology and function [21,144–147]. Other researchers have examined the role of high-resolution ultrasound in guiding gene therapy [148] and in testing efficacy of genetic therapy [149].

6. DISCUSSION AND CONCLUSIONS

Micro-ultrasound has evolved rapidly over the past decade. Mechanical imaging systems that operated at a few frames per second 10 years ago have been replaced by sophisticated array-based machines capable of imaging at hundreds of frames per second and over the full gamut of imaging modes including colour flow, power Doppler and contrast. These instruments fit into the larger scheme of discovery-oriented research across a wide range of applications where small animals such as mice are used to model biological processes and human disease. Today's high-resolution ultrasound instrumentation is already operating close to the limits of performance determined by a consideration of the physics of ultrasound (i.e. upper useful frequencies, transducer apertures and bandwidths, etc). Thus, further improvements in raw spatial and temporal resolution will be difficult to achieve without significant engineering effort. Advanced signal processing and beam-forming methods already demonstrated in lower-frequency ultrasound may have a role in achieving further improvements. For example, coded waveform imaging methods allow for higher frequencies to be used by increasing total signal energy without increasing instantaneous power.

Micro-ultrasound has proved to be a valuable imaging modality for studies in developmental biology when examining normal development and when determining phenotypes caused by genetic alterations or teratogenic agents *in vivo*. Very high resolution enables precise guidance of introduction or extraction of genetic material into early-stage embryos as shown in figure 10. Numerous studies have benefitted from the ability to image the conceptus from within days of implantation to full term of pregnancy. Importantly, Doppler waveforms can be obtained from the day the mouse heart first starts to beat and throughout postnatal development into adulthood facilitating longitudinal haemodynamic studies, and evaluation of long-term cardiovascular outcomes. LV model fitting may assist with 'filling in' gaps arising due to occasionally unavoidable ultrasound signal dropout. Further progress towards a goal of reliable acquisition of a very fine three-dimensional sampling of anatomic data that allows for the development of comprehensive maps of three-dimensional displacements throughout the heart may be anticipated.

Micro-ultrasound makes a unique contribution to the study of cancer models as illustrated in figures 11–15. Two- and three-dimensional imaging of tumour growth with 50–200 μm resolution is a significant improvement over the use of surface callipers for estimating tumour burden. This further enables the growth of orthotopic tumours such as pancreatic carcinoma, spontaneous tumours such as TRAMP (transgenic adenocarcinoma of mouse prostate) and metastasis to be followed in longitudinal studies that would otherwise be impossible to perform. Further, the development of useful contrast imaging integration of micro-ultrasound into experimental protocols enables the initial rapid evaluation of probable drug combinations for cancer therapy. Progress in molecular targeted contrast agents may enable significant progress to be made in understanding the molecular basis of disease and its progression.

In terms of future technological advances, the methodology of micro-ultrasound will be further advanced by the development of photoacoustics and elastography. Development of an integrated platform for high-frequency photoacoustic imaging has recently been reported by Needles *et al.* [150]. This technology may impact cancer research by providing a non-invasive means of evaluating tumour oxygenation. Through the development of nanoparticle-based contrast agents, photoacoustics may also allow the extracellular compartment to be probed. Optical absorption spectroscopy of the tumour microenvironment may allow other new dimensions of tumour growth to be assessed. Shear modulus imaging represents another opportunity to probe fluctuations of elastic properties in tumours as they grow and are treated. The ability to perform this type of imaging at much higher frequencies may reveal new physical properties of tumour tissue.

Finally, it should be noted that micro-ultrasound, having undergone dramatic expansion in the field of preclinical imaging, is now ripe to be exploited in clinical applications. Already efforts are underway to use the technology in prostate imaging, neonatal imaging, skin and ocular imaging and a wide range of intraluminal imaging applications. The development of highly portable versions suitable for anaesthesiology and other clinical activities is to be anticipated.

The authors wish to acknowledge funding from the Terry Fox Foundation, the Canadian Institutes of Health Research, the Ontario Research Fund and VisualSonics. We also wish to thank Dawei Qu for figures 5, 7 and 8 and John Sun for figure 13. We also extend our gratitude to the many staff and graduate students at Sunnybrook and the employees of VisualSonics who helped expand the technology and applications of micro-ultrasound.

REFERENCES

1 Frost & Sullivan. 2010 US preclinical animal imaging systems market. **N5BB-50**, 1–103.
2 Sherar, M. D., Noss, M. B. & Foster, F. S. 1987 Ultrasound backscatter microscopy images the internal structure of living tumour spheroids. *Nature* **330**, 493–495. (doi:10.1038/330493a0)
3 Pavlin, C. J., Harasiewicz, K., Sherar, M. D. & Foster, F. S. 1991 Clinical use of ultrasound biomicroscopy. *Ophthalmology* **98**, 287–295.
4 Pavlin, C. J., Sherar, M. D. & Foster, F. S. 1990 Subsurface imaging of the eye by ultrasound biomicroscopy. *Ophthalmology* **97**, 244–250.
5 Sherar, M. D., Starkoski, B. G., Taylor, W. B. & Foster, F. S. 1989 A 100 MHz B-scan ultrasound backscatter

microscope. *Ultrason. Imag.* **11**, 95–105. (doi:10.1016/0161-7346(89)90002-3)
6 Hoffmann, K., El Gammal, S., Matthes, U. & Altmeyer, P. 1989 Digital 20 MHz sonography of the skin in preoperative diagnosis. *Z. Hautkr.* **64**, 851–852, 5–8.
7 Hoffmann, K., El Gammal, S. & Altmeyer, P. 1990 B-scan ultrasound in dermatology. *Hautarzt* **41**, W7–W16.
8 Bom, N., ten Hoff, H., Lancee, C., Gussenhoven, W. & Bosch, J. 1989 Early and recent intraluminal ultrasound devices. *Int. J. Cardiol. Imag.* **4**, 79–88. (doi:10.1007/BF01745137)
9 Nissen, S., Grines, C., Gurley, J., Sublett, K., Haynie, D., Diaz, C., Booth, D. C. & DeMaria, A. N. 1990 Application of a new phased-array ultrasound imaging catheter in the assessment of vascular dimension: *in vivo* comparison to cineangiography. *Circulation* **81**, 660–666.
10 Yock, P., Linker, D. & Angelsen, B. 1989 Two-dimensional intravascular ultrasound: technical development and initial clinical experience. *J. Am. Soc. Echocardiogr.* **2**, 296–304.
11 Turnbull, D. H., Bloomfield, T. S., Baldwin, H. S., Foster, F. S. & Joyner, A. L. 1995 Ultrasound backscatter microscope analysis of early mouse embryonic brain development. *Proc. Natl Acad. Sci. USA* **92**, 2239–2243. (doi:10.1073/pnas.92.6.2239)
12 Foster, F. S., Pavlin, C. J., Harasiewicz, K. A., Christopher, D. A. & Turnbull, D. H. 2000 Advances in ultrasound biomicroscopy. *Ultrasound Med. Biol.* **26**, 1–27. (doi:10.1016/S0301-5629(99)00096-4)
13 Cobbold, R. 2008 *Foundations of biomedical ultrasound.* New York, NY: Oxford University Press.
14 Foster, F. S. *et al.* 2002 A new ultrasound instrument for *in vivo* microimaging of mice. *Ultrasound Med. Biol.* **28**, 1165–1172. (doi:10.1016/S0301-5629(02)00567-7).
15 Phoon, C. K. 2006 Imaging tools for the developmental biologist: ultrasound biomicroscopy of mouse embryonic development. *Pediatr. Res.* **60**, 14–21. (doi:10.1203/01.pdr.0000219441.28206.79)
16 Zhou, Y. Q., Foster, F. S., Qu, D. W., Zhang, M., Harasiewicz, K. A. & Adamson, S. L. 2002 Applications for multifrequency ultrasound biomicroscopy in mice from implantation to adulthood. *Physiol. Genom.* **10**, 113–126.
17 Nieman, B. J. & Turnbull, D. H. 2010 Ultrasound and magnetic resonance microimaging of mouse development. *Meth. Enzymol.* **476**, 379–400. (doi:10.1016/S0076-6879(10)76021-3)
18 Kulandavelu, S., Qu, D., Sunn, N., Mu, J., Rennie, M. Y., Whiteley, K. J. *et al.* 2006 Embryonic and neonatal phenotyping of genetically engineered mice. *Ilar J.* **47**, 103–117.
19 Pallares, P., Fernandez-Valle, M. E. & Gonzalez-Bulnes, A. 2009 *In vivo* virtual histology of mouse embryogenesis by ultrasound biomicroscopy and magnetic resonance imaging. *Reprod. Fertil. Dev.* **21**, 283–292. (doi:10.1071/RD08124)
20 Li, Y., Garson, C. D., Xu, Y., French, B. A. & Hossack, J. A. 2008 High frequency ultrasound imaging detects cardiac dyssynchrony in noninfarcted regions of the murine left ventricle late after reperfused myocardial infarction. *Ultrasound Med. Biol.* **34**, 1063–1075. (doi:10.1016/j.ultrasmedbio.2007.12.009)
21 Liu, J., Du, J., Zhang, C., Walker, J. W. & Huang, X. 2007 Progressive troponin I loss impairs cardiac relaxation and causes heart failure in mice. *Am. J. Physiol. Heart Circ. Physiol.* **293**, H1273–H1281. (doi:10.1152/ajpheart.01379.2006)
22 Zhou, Y. Q., Foster, F. S., Nieman, B. J., Davidson, L., Chen, X. J. & Henkelman, R. M. 2004 Comprehensive transthoracic cardiac imaging in mice using ultrasound biomicroscopy with anatomical confirmation by magnetic resonance imaging. *Physiol. Genom.* **18**, 232–244.
23 Zhou, Y. Q., Zhu, S. N., Foster, F. S., Cybulsky, M. I. & Henkelman, R. M. 2010 Aortic regurgitation dramatically alters the distribution of atherosclerotic lesions and enhances atherogenesis in mice. *Arterioscler. Thromb. Vasc. Biol.* **30**, 1181–1188. (doi:10.1161/ATVBAHA.110.204198)
24 Cheung, A. M., Brown, A. S., Cucevic, V., Roy, M., Needles, A., Yang, V., Hicklin, D. J., Kerbel, R. S. & Foster, F. S. 2007 Detecting vascular changes in tumour xenografts using micro-ultrasound and micro-CT following treatment with VEGFR-2 blocking antibodies. *Ultrasound Med. Biol.* **33**, 1259–1268. (doi:10.1016/j.ultrasmedbio.2007.01.015)
25 Goessling, W., North, T. E. & Zon, L. I. 2007 Ultrasound biomicroscopy permits *in vivo* characterization of zebrafish liver tumors. *Nat. Meth.* **4**, 551–553. (doi:10.1038/nmeth1059)
26 Graham, K. C., Wirtzfeld, L. A., MacKenzie, L. T., Postenka, C. O., Groom, A. C., MacDonald, I. C., Fenster, A., Lacefield, J. C. & Chambers, A. F. 2005 Three-dimensional high-frequency ultrasound imaging for longitudinal evaluation of liver metastases in preclinical models. *Cancer Res.* **65**, 5231–5237. (doi:10.1158/0008-5472.CAN-05-0440)
27 Olive, K. P. *et al.* 2009 Inhibition of Hedgehog signaling enhances delivery of chemotherapy in a mouse model of pancreatic cancer. *Science* **324**, 1457–1461. (doi:10.1126/science.1171362)
28 Shaked, Y. *et al.* 2006 Therapy-induced acute recruitment of circulating endothelial progenitor cells to tumors. *Science* **313**, 1785–1787. (doi:10.1126/science.1127592)
29 Foster, F. S., Mehi, J., Lukacs, M., Hirson, D., White, C., Chaggares, C. & Needles, A. 2009 A new 15–50 MHz array-based micro-ultrasound scanner for preclinical imaging. *Ultrasound Med. Biol.* **35**, 1700–1708. (doi:10.1016/j.ultrasmedbio.2009.04.012)
30 Borden, M. A., Qin, S. & Ferrara, K. W. 2010 Ultrasound contrast agents. In *Molecular imaging* (ed. R. Weissleder), pp. 425–444. Shelton, CT: Peoples Medical Publishing House.
31 Hamilton, M. F. & Blackstock, D. T. 1998 *Nonlinear acoustics.* New York, NY: Academic Press.
32 Hope Simpson, D., Chin, C. & Burns, P. N. 1999 Pulse inversion Doppler: a new method for detecting nonlinear echoes from microbubble contrast agents. *IEEE Trans. Ultrason. Ferroelectr. Freq. Contr.* **46**, 372–382. (doi:10.1109/58.753026)
33 Burns, P. N., Powers, J. E., Hope Simpson, D., Uhlendorf, V. & Fritzsch, T. 1996 Harmonic imaging: principles and preliminary results. *Angiology* **47**, 63–73.
34 Burns, P. N. & Hope-Simpson, D. 2000 *Pulse inversion Doppler ultrasonic diagnostic imaging.* United States Patent 6,095,980.
35 Haider, B. & Chiao, R. Y. 1999 Higher order nonlinear ultrasonic imaging. In *Proc. IEEE Ultrasonics Symp.*, pp. 1527–1531. (doi:10.1109/ULTSYM.1999.849287)
36 Eckersley, R. J., Chin, C. T. & Burns, P. N. 2005 Optimising phase and amplitude modulation schemes for imaging microbubble contrast agents at low acoustic power. *Ultrasound Med. Biol.* **31**, 213–219. (doi:10.1016/j.ultrasmedbio.2004.10.004)
37 Chomas, J., Dayton, P., May, D. & Ferrara, K. 2002 Nondestructive subharmonic imaging. *IEEE Trans. Ultrason. Ferroelectr. Freq. Contr.* **49**, 883–892. (doi:10.1109/TUFFC.2002.1020158)
38 Forsberg, F., Liu, J. B., Shi, W. T., Furuse, J., Shimizu, M. & Goldberg, B. B. 2005 *In vivo* pressure estimation using

subharmonic contrast microbubble signals: proof of concept. *IEEE Trans. Ultrason. Ferroelectr. Freq. Contr.* **52**, 581–583. (doi:10.1109/TUFFC.2005.1428040)
39 Forsberg, F., Shi, W. T. & Goldberg, B. B. 2000 Subharmonic imaging of contrast agents. *Ultrasonics* **38**, 93–98. (doi:10.1016/S0041-624X(99)00148-1)
40 Shankar, P. M., Krishna, P. D. & Newhouse, V. L. 1999 Subharmonic backscattering from ultrasound contrast agents. *J. Acoust. Soc. Am.* **106**, 2104–2110. (doi:10.1121/1.428142)
41 Shi, W. T., Forsberg, F., Hall, A. L., Chiao, R. Y., Liu, J. B., Miller, S., Thomenius, K. E., Wheatley, M. A. & Goldberg, B. B. 1999 Subharmonic imaging with microbubble contrast agents: initial results. *Ultrason. Imag.* **21**, 79–94.
42 Needles, A., Arditi, M., Rognin, N. G., Mehi, J., Coulthard, T., Bilan-Tracey, C., Gaud, E., Frinking, P., Hirson, D. & Foster, F. S. 2010 Nonlinear contrast imaging with an array-based micro-ultrasound system. *Ultrasound Med. Biol.* **36**, 2097–2106. (doi:10.1016/j.ultrasmedbio.2010.08.012)
43 Serrano, M., Han, M., Brinez, P. & Linask, K. K. 2010 Fetal alcohol syndrome: cardiac birth defects in mice and prevention with folate. *Am. J. Obstet. Gynecol.* **203**, 75 e7–15.
44 McQuinn, T. C., Bratoeva, M., Dealmeida, A., Remond, M., Thompson, R. P. & Sedmera, D. 2007 High-frequency ultrasonographic imaging of avian cardiovascular development. *Dev. Dyn.* **236**, 3503–3513. (doi:10.1002/dvdy.21357)
45 Le Floc'h, J., Cherin, E., Zhang, M. Y., Akirav, C., Adamson, S. L., Vray, D. & Foster, F. S. 2004 Developmental changes in integrated ultrasound backscatter from embryonic blood *in vivo* in mice at high US frequency. *Ultrasound Med. Biol.* **30**, 1307–1319. (doi:10.1016/j.ultrasmedbio.2004.07.018)
46 Foster, F. S., Zhang, M., Duckett, A. S., Cucevic, V. & Pavlin, C. J. 2003 *In vivo* imaging of embryonic development in the mouse eye by ultrasound biomicroscopy. *Invest. Ophthalmol. Vis. Sci.* **44**, 2361–2366. (doi:10.1167/iovs.02-0911)
47 Mu, J., Slevin, J. C., Qu, D., McCormick, S. & Adamson, S. L. 2008 *In vivo* quantification of embryonic and placental growth during gestation in mice using micro-ultrasound. *Reprod. Biol. Endocrinol.* **6**, 34. (doi:10.1186/1477-7827-6-34)
48 Slevin, J. C., Byers, L., Gertsenstein, M., Qu, D., Mu, J., Sunn, N., Kingdom, J. C. P., Rossant, J. & Adamson, S. L. 2006 High resolution ultrasound-guided microinjection for interventional studies of early embryonic and placental development *in vivo* in mice. *BMC Dev. Biol.* **6**, 10. (doi:10.1186/1471-213X-6-10)
49 Ji, R. P., Phoon, C. K., Aristizabal, O., McGrath, K. E., Palis, J. & Turnbull, D. H. 2003 Onset of cardiac function during early mouse embryogenesis coincides with entry of primitive erythroblasts into the embryo proper. *Circ. Res.* **92**, 133–135. (doi:10.1161/01.RES.0000056532.18710.C0)
50 Mu, J. *et al.* 2007 Fgl2 deficiency causes neonatal death and cardiac dysfunction during embryonic and postnatal development in mice. *Physiol. Genom.* **31**, 53–62.
51 Mu, J. & Adamson, S. L. 2006 Developmental changes in hemodynamics of uterine artery, utero- and umbilicoplacental, and vitelline circulations in mouse throughout gestation. *Am. J. Physiol. Heart Circ. Physiol.* **291**, H1421–H1428. (doi:10.1152/ajpheart.00031.2006)
52 Phoon, C. K., Aristizabal, O. & Turnbull, D. H. 2000 40 MHz Doppler characterization of umbilical and dorsal aortic blood flow in the early mouse embryo. *Ultrasound Med. Biol.* **26**, 1275–1283. (doi:10.1016/S0301-5629(00)00278-7)
53 Corrigan, N., Brazil, D. P. & Auliffe, F. M. 2010 High-frequency ultrasound assessment of the murine heart from embryo through to juvenile. *Reprod. Sci.* **17**, 147–157. (doi:10.1177/1933719109348923)
54 Zhou, Y. Q., Foster, F. S., Parkes, R. & Adamson, S. L. 2003 Developmental changes in left and right ventricular diastolic filling patterns in mice. *Am. J. Physiol. Heart Circ. Physiol.* **285**, H1563–H1575.
55 Kulandavelu, S., Qu, D. & Adamson, S. L. 2006 Cardiovascular function in mice during normal pregnancy and in the absence of endothelial NO synthase. *Hypertension* **47**, 1175–1182. (doi:10.1161/01.HYP.0000218440.71846.db)
56 Wong, A. Y., Kulandavelu, S., Whiteley, K. J., Qu, D., Langille, B. L. & Adamson, S. L. 2002 Maternal cardiovascular changes during pregnancy and postpartum in mice. *Am. J. Physiol. Heart Circ. Physiol.* **282**, H918–H925.
57 Adamson, S. L., Lu, Y., Whiteley, K. J., Holmyard, D., Hemberger, M., Pfarrer, C. & Cross, J. 2002 Interactions between trophoblast cells and the maternal and fetal circulation in the mouse placenta. *Dev. Biol.* **250**, 358–373. (doi:10.1006/dbio.2002.0773)
58 Laissue, P. *et al.* 2009 Identification of quantitative trait loci responsible for embryonic lethality in mice assessed by ultrasonography. *Int. J. Dev. Biol.* **53**, 623–629. (doi:10.1387/ijdb.082613pl)
59 Phoon, C. K., Ji, R. P., Aristizabal, O., Worrad, D. M., Zhou, B., Baldwin, H. S. & Turnbull, D. H. 2004 Embryonic heart failure in NFATc1−/− mice: novel mechanistic insights from *in utero* ultrasound biomicroscopy. *Circ. Res.* **95**, 92–99. (doi:10.1161/01.RES.0000133681.99617.28)
60 Nomura-Kitabayashi, A. *et al.* 2009 Outflow tract cushions perform a critical valve-like function in the early embryonic heart requiring BMPRIA-mediated signaling in cardiac neural crest. *Am. J. Physiol. Heart Circ. Physiol.* **297**, H1617–H1628. (doi:10.1152/ajpheart.00304.2009)
61 Lickert, H. *et al.* 2004 Baf60c is essential for function of BAF chromatin remodelling complexes in heart development. *Nature* **432**, 107–112. (doi:10.1038/nature03071)
62 Tada, T. & Kishimoto, H. 1990 Ultrastructural and histological studies on closure of the mouse ductus arteriosus. *Acta Anat.* (*Basel*) **139**, 326–334. (doi:10.1159/000147020)
63 Meyer, K. & Lubo, Z. 2007 Fetal programming of cardiac function and disease. *Reprod. Sci.* **14**, 209–216. (doi:10.1177/1933719107302324)
64 Brown, A. S., Reid, A. D., Leamen, L., Cucevic, V. & Foster, F. S. 2004 Biological effects of high-frequency ultrasound exposure during mouse organogenesis. *Ultrasound Med. Biol.* **30**, 1223–1232. (doi:10.1016/j.ultrasmedbio.2004.07.020)
65 Hande, M. P. & Devi, P. U. 1993 Effect of *in utero* exposure to diagnostic ultrasound on the postnatal survival and growth of mouse. *Teratology* **48**, 405–411. (doi:10.1002/tera.1420480504)
66 Suresh, R., Ramesh Rao, T., Davis, E. M., Ovchinnikov, N. & Mc Rae, A. 2008 Effect of diagnostic ultrasound during the fetal period on learning and memory in mice. *Ann. Anat.* **190**, 37–45. (doi:10.1016/j.aanat.2007.04.008)
67 Mazze, R. I., Wilson, A. I., Rice, S. A. & Baden, J. M. 1985 Fetal development in mice exposed to isoflurane. *Teratology* **32**, 339–345. (doi:10.1002/tera.1420320303)
68 Shah, S. R. *et al.* 2011 Embryonic mouse blood flow and oxygen correlate with early pancreatic differentiation. *Dev. Biol.* **349**, 342–349. (doi:10.1016/j.ydbio.2010.10.033)

69 Beronja, S., Livshits, G., Williams, S. & Fuchs, E. 2010 Rapid functional dissection of genetic networks via tissue-specific transduction and RNAi in mouse embryos. *Nat. Med.* **16**, 821–827. (doi:10.1038/nm.2167)

70 Punzo, C. & Cepko, C. L. 2008 Ultrasound-guided *in utero* injections allow studies of the development and function of the eye. *Dev. Dyn.* **237**, 1034–1042. (doi:10.1002/dvdy.21500)

71 Ellis, L. M. & Hicklin, D. J. 2008 VEGF-targeted therapy: mechanisms of anti-tumour activity. *Nat. Rev. Cancer* **8**, 579–591. (doi:10.1038/nrc2403)

72 Ferrara, N. & Kerbel, R. S. 2005 Angiogenesis as a therapeutic target. *Nature* **438**, 967–974. (doi:10.1038/nature04483)

73 Gore, M. E. *et al.* 2009 Safety and efficacy of sunitinib for metastatic renal-cell carcinoma: an expanded-access trial. *Lancet Oncol.* **10**, 757–763. (doi:10.1016/S1470-2045(09)70162-7)

74 Motzer, R. J. *et al.* 2009 Overall survival and updated results for sunitinib compared with interferon alfa in patients with metastatic renal cell carcinoma. *J. Clin. Oncol.* **27**, 3584–3590. (doi:10.1200/JCO.2008.20.1293)

75 Shojaei, F. & Ferrara, N. 2007 Antiangiogenic therapy for cancer: an update. *Cancer J.* **13**, 345–348. (doi:10.1097/PPO.0b013e31815a7b69)

76 Feldmann, G. *et al.* 2008 An orally bioavailable small-molecule inhibitor of Hedgehog signaling inhibits tumor initiation and metastasis in pancreatic cancer. *Mol. Cancer Ther.* **7**, 2725–2735. (doi:10.1158/1535-7163.MCT-08-0573)

77 Wirtzfeld, L. A. *et al.* 2005 A new three-dimensional ultrasound microimaging technology for preclinical studies using a transgenic prostate cancer mouse model. *Cancer Res.* **65**, 6337–6345. (doi:10.1158/0008-5472.CAN-05-0414)

78 Wang, X. F. *et al.* 2007 A peptide conjugate of vitamin E succinate targets breast cancer cells with high ErbB2 expression. *Cancer Res.* **67**, 3337–3344. (doi:10.1158/0008-5472.CAN-06-2480)

79 Cheung, A. M., Brown, A. S., Hastie, L. A., Cucevic, V., Roy, M., Lacefield, J. C., Fenster, A. & Foster, F. 2005 Three-dimensional ultrasound biomicroscopy for xenograft growth analysis. *Ultrasound Med. Biol.* **31**, 865–870. (doi:10.1016/j.ultrasmedbio.2005.03.003)

80 Balamuth, N. J. *et al.* 2010 Serial transcriptome analysis and cross-species integration identifies centromere-associated protein E as a novel neuroblastoma target. *Cancer Res.* **70**, 2749–2758. (doi:10.1158/0008-5472.CAN-09-3844)

81 DeRosier, L. C. *et al.* 2007 Combination treatment with TRA-8 anti death receptor 5 antibody and CPT-11 induces tumor regression in an orthotopic model of pancreatic cancer. *Clin. Cancer Res.* **13**, 5535s–5543s. (doi:10.1158/1078-0432.CCR-07-1075)

82 Huizen, I. V., Wu, G., Moussa, M., Chin, J. L., Fenster, A., Lacefield, J. C., Sakai, H., Greenberg, N. M. & Xuan, J. W. 2005 Establishment of a serum tumor marker for preclinical trials of mouse prostate cancer models. *Clin. Cancer Res.* **11**, 7911–7919. (doi:10.1158/1078-0432.CCR-05-0953)

83 Kiguchi, K., Ruffino, L., Kawamoto, T., Ajiki, T. & Digiovanni, J. 2005 Chemopreventive and therapeutic efficacy of orally active tyrosine kinase inhibitors in a transgenic mouse model of gallbladder carcinoma. *Clin. Cancer Res.* **11**, 5572–5580. (doi:10.1158/1078-0432.CCR-04-2603)

84 Lyshchik, A., Fleischer, A. C., Huamani, J., Hallahan, D. E., Brissova, M. & Gore, J. C. 2007 Molecular imaging of vascular endothelial growth factor receptor 2 expression using targeted contrast-enhanced high-frequency ultrasonography. *J Ultrasound Med.* **26**, 1575–1586.

85 Wu, G., Wang, L., Yu, L., Wang, H. & Xuan, J. W. 2005 The use of three-dimensional ultrasound micro-imaging to monitor prostate tumor development in a transgenic prostate cancer mouse model. *Tohoku J. Exp. Med.* **207**, 181–189. (doi:10.1620/tjem.207.181)

86 Ayers, G. D. *et al.* 2010 Volume of preclinical xenograft tumors is more accurately assessed by ultrasound imaging than manual caliper measurements. *J. Ultrasound Med.* **29**, 891–901.

87 Goertz, D. E., Yu, J. L., Kerbel, R. S., Burns, P. N. & Foster, F. S. 2002 High-frequency Doppler ultrasound monitors the effects of antivascular therapy on tumor blood flow. *Cancer Res.* **62**, 6371–6375.

88 Jugold, M., Palmowski, M., Huppert, J., Woenne, E. C., Mueller, M. M., Semmler, W. & Kiessling, F. 2008 Volumetric high-frequency Doppler ultrasound enables the assessment of early antiangiogenic therapy effects on tumor xenografts in nude mice. *Eur. Radiol.* **18**, 753–758. (doi:10.1007/s00330-007-0825-5)

89 Xuan, J. W. *et al.* 2007 Functional neoangiogenesis imaging of genetically engineered mouse prostate cancer using three-dimensional power Doppler ultrasound. *Cancer Res.* **67**, 2830–2839. (doi:10.1158/0008-5472.CAN-06-3944)

90 Franco, M., Shan, M., Limor, C., Urban, E., Yuval, S., Cheung, A. M., Brown, A. S., Hicklin, D. J., Foster, F. S. & Kerbel, R. S. 2006 Targeted anti-vascular endothelial growth factor receptor-2 therapy leads to short-term and long-term impairment of vascular function and increase in tumor hypoxia. *Cancer Res.* **66**, 3639–3648. (doi:10.1158/0008-5472.CAN-05-3295)

91 Qayum, N., Muschel, R. J., Im, J. H., Balathasan, L., Koch, C. J., Patel, S., McKenna, W. G. & Bernhard, E. J. 2009 Tumor vascular changes mediated by inhibition of oncogenic signaling. *Cancer Res.* **69**, 6347–6354. (doi:10.1158/0008-5472.CAN-09-0657)

92 Hudson, J. M., Karshafian, R. & Burns, P. N. 2009 Quantification of flow using ultrasound and microbubbles: a disruption replenishment model based on physical principles. *Ultrasound Med. Biol.* **35**, 2007–2020. (doi:10.1016/j.ultrasmedbio.2009.06.1102)

93 Lanza, G. M. *et al.* 1997 High-frequency ultrasonic detection of thrombi with a targeted contrast system. *Ultrasound Med. Biol.* **23**, 863–870. (doi:10.1016/S0301-5629(97)00046-X)

94 Lanza, G. M. *et al.* 1996 A novel site-targeted ultrasonic contrast agent with broad biomedical application. *Circulation* **94**, 3334–3340.

95 Ellegala, D. B., Leong-Poi, H., Carpenter, J. E., Klibanov, A. L., Kaul, S., Shaffrey, M. E., Sklenar, J. & Lindner, J. R. 2003 Imaging tumor angiogenesis with contrast ultrasound and microbubbles targeted to alpha(v)beta3. *Circulation* **108**, 336–341. (doi:10.1161/01.CIR.0000080326.15367.0C)

96 Leong-Poi, H., Christiansen, J., Heppner, P., Lewis, C. W., Klibanov, A. L., Kaul, S. & Lindner, J. R. 2005 Assessment of endogenous and therapeutic arteriogenesis by contrast ultrasound molecular imaging of integrin expression. *Circulation* **111**, 3248–3254. (doi:10.1161/CIRCULATIONAHA.104.481515)

97 Leong-Poi, H., Christiansen, J., Klibanov, A. L., Kaul, S. & Lindner, J. R. 2003 Noninvasive assessment of angiogenesis by ultrasound and microbubbles targeted to alpha(v)-integrins. *Circulation* **107**, 455–460. (doi:10.1161/01.CIR.0000044916.05919.8B)

98 Rychak, J. J., Graba, J., White, C., Cheung, A. M. Y., Mistry, B., Lindner, J. R., Kerbel, R. S. & Foster, F. S. 2007 Micro-ultrasound molecular imaging of VEGFR-2 in a mouse model of tumor angiogenesis. *Mol. Imag.* **6**, 289–296.

99 Willmann, J. K., Paulmurugan, R., Chen, K., Gheysens, O., Rodriguez-Porcel, M., Lutz, A. M., Chen, I. Y., Chen, X. & Gambhir, S. S. 2008 Ultrasonic imaging of tumor angiogenesis with contrast microbubbles targeted to vascular endothelial growth factor receptor 2 in mice. *Radiology* **246**, 508–518. (doi:10.1148/radiol.2462070536)

100 Willmann, J. K., Cheng, Z., Davis, C., Lutz, A. M., Schipper, M. L., Nielsen, C. H. & Gambhir, S. S. 2008 Targeted microbubbles for imaging tumor angiogenesis: assessment of whole-body biodistribution with dynamic micro-PET in mice. *Radiology* **249**, 212–219. (doi:10.1148/radiol.2491072050)

101 Willmann, J. K., Lutz, A. M., Paulmurugan, R., Patel, M. R., Chu, P., Rosenberg, J. & Gambhir, S. S. 2008 Dual-targeted contrast agent for US assessment of tumor angiogenesis *in vivo*. *Radiology* **248**, 936–944. (doi:10.1148/radiol.2483072231)

102 Pysz, M. A., Foygel, K., Rosenberg, J., Gambhir, S. S., Schneider, M. & Willmann, J. K. 2010 Antiangiogenic cancer therapy: monitoring with molecular US and a clinically translatable contrast agent (BR55). *Radiology* **256**, 519–527. (doi:10.1148/radiol.10091858)

103 Carmeliet, P. & Collen, D. 2000 Transgenic mouse models in angiogenesis and cardiovascular disease. *J. Pathol.* **190**, 387–405. (doi:10.1002/(SICI)1096-9896(200002)190:3<387::AID-PATH595>3.0.CO;2-R)

104 Michael, L. H., Entman, M. L., Hartley, C. J., Youker, K. A., Zhu, J., Hall, S. R., Hawkins, H. K., Berens, H. K. & Ballantyne, C. M. 1995 Myocardial ischemia and reperfusion: a murine model. *Am. J. Physiol.* **269**, H2147–H2154.

105 Michael, L. *et al.* 1999 Myocardial infarction and remodeling in mice: effect of reperfusion. *Am. J. Physiol.* **277**, H660–H668.

106 Guo, Y., Wu, W. J., Qiu, Y., Tang, X. L., Yang, Z. & Bolli, R. 1998 Demonstration of an early and a late phase of ischemic preconditioning in mice. *Am. J. Physiol.* **275**, H1375–H1387.

107 Tarnavski, O. 2009 Mouse surgical models in cardiovascular research. *Meth. Mol. Biol.* **573**, 115–137. (doi:10.1007/978-1-60761-247-6_7)

108 Yang, X. P., Liu, Y. H., Rhaleb, N. E., Kurihara, N., Kim, H. E. & Carretero, O. A. 1999 Echocardiographic assessment of cardiac function in conscious and anesthetized mice. *Am. J. Physiol.* **277**, H1967–H1974.

109 Scherrer-Crosbie, M. & Kurtz, B. 2010 Ventricular remodeling and function: insights using murine echocardiography. *J. Mol. Cell. Cardiol.* **48**, 512–517. (doi:10.1016/j.yjmcc.2009.07.004)

110 Bylund, N., Andersson, M. & Knutsson, H. 2005 Interactive 3D filter design for ultrasound artifact reduction. In *Proc. IEEE Int. Conf. on Image Processing*, vol. 3, pp. 728–731. (doi:10.1109/ICIP.2005.1530495)

111 Mauldin, F., Lin, D. & Hossack, J. In press. A singular value filter for rejection of stationary artifact in medical ultrasound. In *Proc. 2010 IEEE Ultrasonics Symp.*

112 Li, Y., Garson, C. D., Xu, Y., Beyers, R. J., Epstein, F. H., French, B. A. & Hossack, J. 2007 Quantification and MRI validation of regional contractile dysfunction in mice post myocardial infarction using high resolution ultrasound. *Ultrasound Med. Biol.* **33**, 894–904. (doi:10.1016/j.ultrasmedbio.2006.12.008)

113 Luo, J., Fujikura, K. & Konofagou, E. 2006 Detection of murine infarcts using myocardial elastography at both high temporal and spatial resolution. In *Proc. 28th Int. Conf. IEEE Engineering in Medicine and Biology Society*, pp. 1552–1555. (doi:10.1109/IEMBS.2006.259868)

114 Luo, J., Fujikura, K., Homma, S. & Konofagou, E. 2007 Automated contour tracking for myocardial elastography *in vivo*. In *Proc. 4th IEEE Int. Symp. on Biomedical Imaging: from Nano to Macro*, pp. 952–955. (doi:10.1109/ISBI.2007.357011)

115 Luo, J., Fujikura, K., Homma, S. & Konofagou, E. 2007 Myocardial elastography at both high temporal and spatial resolution for the detection of infarcts. *Ultrasound Med. Biol.* **33**, 1206–1223. (doi:10.1016/j.ultrasmedbio.2007.01.019)

116 Garson, C. D., Li, Y. & Hossack, J. A. 2008 3D cardiac motion estimation using RF signal decorrelation. In *Proc. IEEE Ultrasonics Symp.*, pp. 471–474. (doi:10.1109/ULTSYM.2008.0115)

117 Pernot, M. & Konofagou, E. E. 2005 Electromechanical imaging of the myocardium at normal and pathological states. In *Proc. IEEE Ultrasonics Symp.*, pp. 1091–1094. (doi:10.1109/ULTSYM.2005.1603040)

118 Pernot, M., Fujikura, K., Fun-Kee-Fung, S. & Konofagou, E. 2007 ECG-gated, mechanical and electromechanical wave imaging of cardiovascular tissues *in vivo*. *Ultrasound Med. Biol.* **33**, 1075–1085. (doi:10.1016/j.ultrasmedbio.2007.02.003)

119 Williams, R., Needles, A., Cherin, E., Zhou, Y., Henkelman, R., Adamson, S. & Foster, F. 2007 Noninvasive ultrasonic measurement of regional and local pulse-wave velocity in mice. *Ultrasound Med. Biol.* **33**, 1368–1375. (doi:10.1016/j.ultrasmedbio.2007.03.012)

120 Fujikura, K., Luo, J., Pernot, M., Fukumoto, R., Iii, D. T. & Konofagou, E. E. 2006 Pulse wave imaging in murine abdominal aortas. In *Proc. IEEE Ultrasonics Symp.*, pp. 868–871. (doi:10.1109/ULTSYM.2006.232)

121 Pitzalis, M. V., Iacoviello, M., Romito, R., Guida, P., De Tommasi, E., Luzzi, G., Anaclerio, M., Forleio, C. & Rizzon, P. 2005 Ventricular asynchrony predicts a better outcome in patients with chronic heart failure receiving cardiac resynchronization therapy. *J. Am. Coll. Cardiol.* **45**, 70–71.

122 Li, Y., Garson, C., Xu, Y., French, B. & Hossack, J. 2008 High frequency ultrasound imaging detects cardiac dyssynchrony in noninfarcted regions of the murine left ventricle late after reperfused myocardial infarction. *Ultrasound Med. Biol.* **34**, 1063–1075. (doi:10.1016/j.ultrasmedbio.2007.12.009)

123 Scherrer-Crosbie, M., Rodrigues, A. C., Hataishi, R. & Picard, M. H. 2007 Infarct size assessment in mice. *Echocardiography* **24**, 90–96.

124 French, B., Li, Y., Klibanov, A., Yang, Z. & Hossack, J. 2006 *3D perfusion mapping in post-infarct mice using myocardial contrast echocardiography.* New York, NY: Elsevier.

125 Wei, K., Jayaweera, A. R., Firoozan, S., Linka, A., Skyba, D. M. & Kaul, S. 1998 Quantification of myocardial blood flow with ultrasound-induced destruction of microbubbles administered as a constant venous infusion. *Circulation* **97**, 473–483.

126 Kaufmann, B., Lankford, M., Behm, C., French, B., Klibanov, A., Xu, Y. & Lindner, J. R. 2007 High-resolution myocardial perfusion imaging in mice with high-frequency echocardiographic detection of a depot contrast agent. *J. Am. Soc. Echocardiogr.* **20**, 136–143.

127 Bloch, S. H., Dayton, P. A. & Ferrara, K. W. 2004 Targeted imaging using ultrasound contrast agents. Progess and opportunities for clinical and research applications. *IEEE Eng. Med. Biol. Mag.* **23**, 18–29. (doi:10.1109/MEMB.2004.1360405)

128 Klibanov, A. L., Rasche, P. T., Hughes, M. S., Wojdyla, J. K., Galen, K. P., Wible, J. H. & Brandenburger, G. H. 2004 Detection of individual microbubbles of ultrasound contrast agents: imaging of free-floating and targeted bubbles. *Invest. Radiol.* **39**, 187–195. (doi:10.1097/01.rli.0000115926.96796.75)

129 Lindner, J., Song, J., Christiansen, J., Klibanov, A., Xu, F. & Ley, K. 2001 Ultrasound assessment of inflammation and renal tissue injury with microbubbles targeted to P-selectin. *Circulation* **104**, 2107–2112. (doi:10.1161/hc4201.097061)

130 Takalkar, A., Klibanov, A., Rychak, J., Lindner, J. & Ley, K. 2004 Binding and detachment dynamics of microbubbles targeted to P-selectin under controlled shear flow. *J. Controlled Release* **96**, 473–482. (doi:10.1016/j.jconrel.2004.03.002)

131 Villanueva, F. S., Jankowski, R. J., Klibanov, S., Pina, M. L., Alber, S. M., Watkins, S. C., Brandenburger, G. H. & Wagner, W. R. 1998 Microbubbles targeted to intercellular adhesion molecule-1 bind to activated coronary artery endothelial cells. *Circulation* **98**, 1–5.

132 Kaufmann, B. A., Sanders, J. M., Davis, C., Xie, A., Aldred, P., Sarembock, I. J. & Lindner, J. R. 2007 Molecular imaging of inflammation in atherosclerosis with targeted ultrasound detection of vascular cell adhesion molecule-1. *Circulation* **116**, 276–284. (doi:10.1161/CIRCULATIONAHA.106.684738)

133 Kaufmann, B. A. & Lindner, J. R. 2007 Molecular imaging with targeted contrast ultrasound. *Curr. Opin. Biotechnol.* **18**, 11–16. (doi:10.1016/j.copbio.2007.01.004)

134 Klibanov, A. L., Rychak, J. J., Yang, W. C., Alikhani, S., Li, B., Acton, S., Lindner, J. R., Ley, K. & Kaul, S. 2006 Targeted ultrasound contrast agent for molecular imaging of inflammation in high-shear flow. *Contrast Media Mol. Imag.* **1**, 259–266. (doi:10.1002/cmmi.113)

135 Klibanov, A. L. 2004 Ligand-carrying gas-filled microbubbles: ultrasound contrast agents for targeted molecular imaging. *Bioconj. Chem.* **16**, 9–17.

136 Klibanov, A. L. 2006 Microbubble contrast agents: targeted ultrasound imaging and ultrasound-assisted drug-delivery applications. *Invest. Radiol.* **41**, 354–362. (doi:10.1097/01.rli.0000199292.88189.0f)

137 Phillips, L. C., Klibanov, A. L., Bowles, D. K., Ragosta, M., Hossack, J. A. & Wamhoff, B. R. 2010 Focused *in vivo* delivery of plasmid DNA to the porcine vascular wall via intravascular ultrasound destruction of microbubbles. *J. Vasc. Res.* **47**, 270–274. (doi:10.1159/000258905)

138 Patten, R. D., Aronovitz, M. J., Bridgman, P. & Pandian, N. G. 2002 Use of pulse wave and color flow Doppler echocardiography in mouse models of human disease. *J. Am. Soc. Echocardiogr.* **15**, 708–714. (doi:10.1067/mje.2002.118912)

139 Collins, K. A., Korcarz, C. E. & Lang, R. M. 2003 Use of echocardiography for the phenotypic assessment of genetically altered mice. *Physiol. Genom.* **13**, 227–239.

140 Hartley, C. J., Taffet, G. E., Michael, L. H., Pham, T. T. & Entman, M. L. 1997 Noninvasive determination of pulse-wave velocity in mice. *Am. J. Physiol. Heart Circ. Physiol.* **273**, H494–H500.

141 Zhou, Y. Q., Zhu, S. N., Foster, F. S., Cybulsky, M. I. & Henkelman, R. M. 2010 Aortic regurgitation dramatically alters the distribution of atherosclerotic lesions and enhances atherogenesis in mice. *Arterioscler. Thromb. Vasc. Biol.* **30**, 1181–1188. (doi:10.1161/ATVBAHA.110.204198)

142 Kanashiro-Takeuchi, R. M. *et al.* 2010 Cardioprotective effects of growth hormone-releasing hormone agonist after myocardial infarction. *Proc. Natl Acad. Sci. USA* **107**, 2604–2609. (doi:10.1073/pnas.0914138107)

143 Shamhart, P. E., Luther, D. J., Hodson, B. R., Koshy, J. C., Ohanyan, V. & Meszaros, J. G. 2009 Impact of type 1 diabetes on cardiac fibroblast activation: enhanced cell cycle progression and reduced myofibroblast content in diabetic myocardium. *Am. J. Physiol. Endocrinol. Metab.* **297**, E1147–E1153. (doi:10.1152/ajpendo.00327.2009)

144 Spinale, F. G. *et al.* 2009 Cardiac-restricted overexpression of membrane type-1 matrix metalloproteinase in mice: effects on myocardial remodeling with aging. *Circ. Heart Fail.* **2**, 351–360. (doi:10.1161/CIRCHEARTFAILURE.108.844845)

145 Phoon, C. K. L. & Turnbull, D. H. 2003 Ultrasound biomicroscopy: Doppler in mouse cardiovascular development. *Physiol. Genom.* **14**, 3–15.

146 Barrick, C. J., Dong, A., Waikel, R., Corn, D., Yang, F., Threadgill, D. W. & Smyth, S. S. 2009 Parent-of-origin effects on cardiac response to pressure overload in mice. *Am. J. Physiol. Heart Circ. Physiol.* **297**, H1003–H1009. (doi:10.1152/ajpheart.00896.2008)

147 Kayama, Y. *et al.* 2009 Cardiac 12/15 lipoxygenase-induced inflammation is involved in heart failure. *J. Exp. Med.* **206**, 1565–1574. (doi:10.1084/jem.20082596)

148 Rodriguez-Porcel, M., Gheysens, O., Chen, I., Wu, J. & Gambhir, S. 2005 Image-guided cardiac cell delivery using high-resolution small-animal ultrasound. *Mol. Ther.* **12**, 1142–1147. (doi:10.1016/j.ymthe.2005.07.532)

149 Pleger, S. *et al.* 2005 S100A1 gene therapy preserves *in vivo* cardiac function after myocardial infarction. *Mol. Ther.* **12**, 1120–1129. (doi:10.1016/j.ymthe.2005.08.002)

150 Needles, A., Heinmiller, A., Ephrat, P., Bilan-Tracey, C., Trujillo, A., Theodoropoulos, C., Hirson, D. & Foster, F. S. In press. Development of a combined photoacoustic micro-ultrasound system for estimating blood oxygenation. In *Proc. 2010 IEEE Ultrasonics Symp.*